Development 140, 3176-3187 (2013) doi:10.1242/dev.092502

Tbx20 acts upstream of Wnt signaling to regulate endocardial cushion formation and valve remodeling during mouse cardiogenesis

Xiaoqiang Cai[1], Weijia Zhang[2], Jun Hu[1], Lu Zhang[1], Nishat Sultana[1], Bingruo Wu[3], Weibin Cai[1], Bin Zhou[3] and Chen-Leng Cai[1,*]

SUMMARY

Cardiac valves are essential to direct forward blood flow through the cardiac chambers efficiently. Congenital valvular defects are prevalent among newborns and can cause an immediate threat to survival as well as long-term morbidity. Valve leaflet formation is a rigorously programmed process consisting of endocardial epithelial-mesenchymal transformation (EMT), mesenchymal cell proliferation, valve elongation and remodeling. Currently, little is known about the coordination of the diverse signals that regulate endocardial cushion development and valve elongation. Here, we report that the T-box transcription factor *Tbx20* is expressed in the developing endocardial cushions and valves throughout heart development. Ablation of *Tbx20* in endocardial cells causes severe valve elongation defects and impaired cardiac function in mice. Our study reveals that endocardial Tbx20 is crucial for valve endocardial cell proliferation and extracellular matrix development, but is not required for initiation of EMT. Elimination of *Tbx20* also causes aberrant Wnt/β-catenin signaling in the endocardial cushions. In addition, Tbx20 regulates *Lef1*, a key transcriptional mediator for Wnt/β-catenin signaling, in this developmental process. Our study suggests a model in which Tbx20 regulates the Wnt pathway to direct endocardial cushion maturation and valve elongation, and provides new insights into the etiology of valve defects in humans.

KEY WORDS: Heart development, Cardiac valve, Mouse, Tbx20

INTRODUCTION

Cardiac valves are highly organized, yet delicate structures that ensure unidirectional blood flow through the cardiac chambers and large vessels. Proper formation of the cardiac valves is crucial for normal heart function. Disturbed development of the cardiac valves leads to aberrant heart formation and function, accounting for a large proportion (~25-30%) of congenital heart disease (CHD) in humans (Armstrong and Bischoff, 2004).

The formation of cardiac valves is a dynamic process achieved by a series of complex events including lineage determination, cell proliferation, differentiation and migration. In mammals, the endothelium within the early bilateral heart tube gives rise to the first endocardial cells (Armstrong and Bischoff, 2004). Cardiac valve formation begins with the specification of these endocardial cells (Chakraborty et al., 2010). At embryonic day (E) 9.5-10.5 in mice, endocardium within the atrioventricular canal (AVC) and outflow tract (OFT) gives rise to cushion mesenchymal cells through epithelial-mesenchymal transformation (EMT). These mesenchymal cells subsequently migrate into the cardiac jelly secreted by the overlying myocardial cells to form the endocardial cushions (Person et al., 2005). Between E11.5 and E12.5, cushion mesenchyme undergoes rapid expansion to generate the tissues required for subsequent valve leaflet formation (Person et al., 2005); even at this early stage, the primitive valves are crucial for normal cardiac function. As gestation progresses (E12.5-17.5), the primitive valves elongate and are remodeled to transition from valve primordia to mature valve leaflets (Chakraborty et al., 2010).

The signaling cascades that regulate EMT initiation and mesenchymal cell proliferation during early valve development have been extensively studied (Person et al., 2005). Transcription factors and growth factors in the endocardium and myocardium (Person et al., 2005), as well as the extracellular matrix (ECM) in the cardiac jelly (Hinton et al., 2006), act cooperatively to initiate EMT and mesenchymal cell proliferation. It is far less clear, however, how these diverse signals are integrated to instruct valve elongation and remodeling. Previous studies revealed that Nfatc1, a transcription factor specifically expressed in the endocardium during early cardiogenesis, is required for valve elongation (Chang et al., 2004; de la Pompa et al., 1998; Ranger et al., 1998). Further studies showed that Nfatc1 regulates endocardial cell fate in the allocation of endocardial cells to EMT and valve elongation (Wu et al., 2011). VEGFs also regulate leaflet morphogenesis (Stankunas et al., 2010). The importance of BMP family members in this process is evident from the findings that endocardial deletion of *Bmpr2* or *Cxcr7* results in thickened valve leaflets (Beppu et al., 2009; Yu et al., 2011) and that *Ltbp1L* (long form of latent TGFβ binding protein 1) null mice exhibit late stage valve hyperplasia (Todorovic et al., 2011). Cardiac neural crest Pax3 and FGF/BMP signals also mediate the differentiation, remodeling and function of OFT semilunar valves (Jain et al., 2011; Zhang et al., 2010). In addition, both ECM content [e.g. periostin (Postn)] and ECM remodeling play important roles in leaflet development (Dupuis et al., 2011; Kruithof et al., 2007; Snider et al., 2008).

[1]Department of Developmental and Regenerative Biology, The Mindich Child Health and Development Institute, and The Black Family Stem Cell Institute, Icahn School of Medicine at Mount Sinai, New York, NY 10029, USA. [2]Renal Division of the Department of Medicine, Icahn School of Medicine at Mount Sinai, New York, NY 10029, USA. [3]Departments of Genetics, Pediatrics and Medicine (Cardiology), Albert Einstein College of Medicine of Yeshiva University, Bronx, NY 10461, USA.

*Author for correspondence (chenleng.cai@mssm.edu)

Accepted 16 May 2013

T-box (Tbx) genes encode transcription factors that are essential for proper organogenesis (Naiche et al., 2005). Mutations of T-box genes cause diverse genetic disorders in humans (Packham and Brook, 2003). *Tbx20* is an ancient T-box family member whose expression in the heart is highly conserved across species (Griffin et al., 2000; Iio et al., 2001; Kraus et al., 2001; Meins et al., 2000). Previous studies showed that *Tbx20* null (*Tbx20*$^{-/-}$) mice die at E9.5-10.5 with severely hypoplastic myocardial tubes (Cai et al., 2005; Singh et al., 2005; Stennard et al., 2005). By contrast, *Tbx20* knockdown mice exhibit failed OFT septation and hypoplastic right ventricle (Takeuchi et al., 2005). Tbx20 is also expressed in the avian endocardial cushions and promotes cushion mesenchymal cell proliferation and ECM gene expression *in vitro* (Shelton and Yutzey, 2007). In addition, myocardial Tbx20 is crucial for early AVC formation and EMT initiation through activation of *Bmp2* in mice (Cai et al., 2011). The role of Tbx20 in valve elongation and remodeling in mammals is largely unknown. These are imperative questions as human *TBX20* mutations cause CHD with defective valvulogenesis (Kirk et al., 2007; Qian et al., 2008).

In this study, we evaluated *Tbx20* expression with *Tbx20*$^{nlacZ/H2BGFP}$ knock-in mice and found that *Tbx20* is dynamically expressed in developing valves, including the early cushion endocardium, cushion mesenchyme and mature valve leaflets. To determine whether Tbx20 is required in the endothelium for valve development, we eliminated *Tbx20* by crossing *Tbx20* floxed mice to an endocardial-specific *Cre* mouse, *Nfatc1*$^{Cre/+}$ (Wu et al., 2012). Our data indicate that endocardial Tbx20 expression is not essential for EMT initiation but is crucial for endocardial cushion maturation and valve elongation. Tbx20 regulates *Lef1*, a crucial transcriptional mediator for the Wnt/β-catenin pathways, in the cushion endocardial cells. Disruption of *Tbx20* results in aberrant Wnt/β-catenin signaling in the endocardial cushions. Our data reveal a previously unknown genetic program of valve development in mammals, thereby providing new insights into the etiology of human congenital valve defects.

MATERIALS AND METHODS

Animals

Tbx20 floxed (*Tbx20*$^{flox/flox}$ or *Tbx20*$^{f/f}$) and heterozygous mice (*Tbx20*$^{+/-}$) were described previously (Cai et al., 2005). *Nfatc1:Cre* (*Nfatc1*$^{Cre/+}$) knock-in mice were reported recently (Wu et al., 2012). For *Tbx20:nlacZ/H2BGFP* (*Tbx20*$^{nlacZ/H2BGFP}$) mice, a *LoxP-nlacZ-polyA-LoxP-H2BGFP-polyA* cassette was introduced into the *Tbx20* genomic locus (6 bp upstream of the ATG, with removal of exon 1 coding sequences). Mice derived from the positive embryonic stem cells (ESCs) were crossed to *Flippase* mice (Farley et al., 2000) to remove the *Neo* cassette. *Tbx20:H2BGFP* (*Tbx20*^{H2BGFP}) mice were obtained by crossing *Tbx20*$^{nlacZ/H2BGFP}$ to *Protamine-Cre* mice (O'Gorman et al., 1997) to excise the *nlacZ-polyA* fragment (supplementary material Fig. S1). *TOPGAL* transgenic indicator mice were obtained from the Jackson Laboratory (DasGupta and Fuchs, 1999). The *Tbx20*$^{V5-Avi}$ biotin tag knock-in mouse was generated as illustrated in Fig. 6T. In brief, *V5* and *Avi* tags were fused to *Tbx20* full-length cDNA at the 5′ and 3′ ends, respectively. The fusion cassette (*V5-Tbx20-Avi*) was inserted into the *Tbx20* genomic locus through gene targeting (replacing exon 1 coding sequences). Mice derived from the positive ESCs were crossed to *Rosa26*^{BirA} mice (Driegen et al., 2005). *Tbx20*$^{V5\text{-}Avi/V5\text{-}Avi}$;*Rosa26*$^{BirA/BirA}$ doubly homozygous mice were viable and normal (indistinguishable in development and appearance from wild type). All mice were bred in a mixed genetic background (Black Swiss). Experiments involving animals were carried out according to an approved protocol from the Institutional Animal Care and Use Committee at the Icahn School of Medicine at Mount Sinai, and were in compliance with the NIH animal welfare guidelines.

RNA *in situ* hybridization and histology

Whole-mount RNA *in situ* hybridization of mouse embryos was carried out as described (Wilkinson, 1992). Section RNA *in situ* hybridization was carried out on 12 μm cryosections. For histology, mouse embryos were fixed in 4% paraformaldehyde, dehydrated through an ethanol gradient and embedded in wax using a standard procedure. Paraffin sections were cut at 8 μm and stained with Hematoxylin and Eosin (H&E) as required.

X-Gal and Alcian Blue staining

For whole-mount X-Gal staining, mouse embryos were fixed in 4% paraformaldehyde for 30-40 minutes. After permeabilization (0.02% sodium deoxycholate, 0.01% NP40 in PBS), embryos were stained in X-Gal solution (5 mM potassium ferricyanide, 5 mM potassium ferrocyanide, 2 mM $MgCl_2$, 1 mg/ml X-Gal in PBS) for 12 hours. For X-Gal staining on sections, mouse embryos were fixed, dehydrated and embedded in OCT Compound (Sakura). Cryosections were then stained in X-Gal staining solution. For Alcian Blue staining, tissue paraffin sections were rehydrated and stained in 3% Alcian Blue solution (pH 2.5) for 30 minutes. Sections were then washed in tap water and counterstained with Nuclear Fast Red using a standard procedure (Bancroft and Gamble, 2008).

Immunohistochemistry and imaging

Mouse embryos were fixed in 4% paraformaldehyde and embedded in OCT Compound. Cryosections were cut at 8 μm. The following primary antibodies were used: rabbit anti-Tbx20 (1:100, Sigma), rabbit anti-Mmp13 (1:150, Abcam), mouse anti-Acan (1:150, Millipore), chicken anti-GFP (1:1000, Abcam), mouse anti-Nfatc1 (1:100, Abcam), rat anti-CD31 (1:500, BD Biosciences), mouse MF20 (anti-myosin heavy chain monoclonal; 1:100, DSHB) and rabbit anti-Lef1 (1:100, Cell Signaling). Secondary antibodies, including rabbit anti-chicken DyLight 488 (Abcam), donkey anti-mouse Alexa Fluor 594, donkey anti-rat Alexa Fluor 594 and donkey anti-rabbit Alexa Fluor 488 (Invitrogen), were diluted at 1:200 in blocking solution. DAPI was applied to detect nuclei.

Echocardiography

Pregnant female mice were lightly anesthetized with 0.5-1% isoflurane and the uterus was exposed. *In utero* echocardiography was performed using a high-resolution micro-ultrasound system (VisualSonics Vevo770) with a 30 MHz transducer (RMV-710). Doppler echocardiography was performed to detect blood flow through the aortic valves of the embryos. After imaging, the embryos were harvested for genotyping.

Measurements of relative cushion size and valve length

Comparable sections from mutant and control embryos were stained with H&E and then photographed using a Leica DM5500B microscope. For E11.5-12.5 hearts, cushion and ventricular chamber sizes from each section were measured in arbitrary units using Adobe Photoshop CS2. The cushion size ratio was determined by dividing the raw size of cushions by the raw size of the left ventricle to minimize the effect of developmental stage variation among the embryos. Relative cushion sizes were calculated by dividing the cushion size ratio of mutant embryos by that of control littermates (Jiao et al., 2006). For E14.5 hearts, the raw length of the valve leaflet was measured, and the relative valve length was determined by dividing the raw length of mutant embryos by that of control littermates (Stankunas et al., 2010). A minimum of four mutants and four control littermates were examined at each stage. Student's *t*-test was conducted to examine the difference between the two groups. $P<0.05$ was considered significant.

Cell proliferation and apoptosis assays

EdU (5-ethynyl-2′-deoxyuridine) was dissolved in PBS and injected intraperitoneally into timed pregnant mice (0.5 mg per 100 g body weight) 2 hours prior to harvesting. Embryos were fixed in 4% paraformaldehyde for 1 hour at 4°C, and embedded in paraffin for sectioning. Immunodetection of proliferative cells was performed using the Click-iT EdU Cell Proliferation Assay Kit (Invitrogen). Apoptotic cells were detected with the *In Situ* Cell Death Detection Kit (Roche).

High-throughput mRNA sequencing (mRNA-Seq) and data analysis

Total RNA was isolated from E12.5 hearts with Trizol (Invitrogen). mRNA and cDNA library preparation was performed using an mRNA-Seq Sample Preparation Kit (Illumina) according to the manufacturer's protocol. Next-generation sequencing was performed using a HiSeq 2000 (Illumina). The clean reads from the Illumina pipeline were aligned to the mouse reference genome (mm9), RefSeq exons, splicing junctions and contamination databases (including ribosome and mitochondrial sequences) using the Burrows-Wheeler Aligner (BWA). After filtering reads mapped to contamination databases, the reads uniquely aligned to exons and splicing junction sites with a maximum of two mismatches for each RefSeq transcript were counted to represent the overall expression level of the corresponding transcript. To compare the expression levels of transcripts between samples, read counts were normalized by multiplying a factor of the maximum of the total read counts in all samples by the total read counts in the corresponding sample, and the $\log_2$ ratios were calculated based on normalized counts. Differentially expressed transcripts were identified using the M-A-based random sampling method implemented in the DEGseq package in BioConductor (http://bioconductor.org/packages/2.5/bioc/html/DEGseq.html). The transcripts were further filtered at >1.5-fold change and a minimum read count of 100 in either condition. Significant Gene Ontology (GO) terms were identified in differentially expressed genes using the Database for Annotation, Visualization and Integrated Discovery (DAVID) (National Institute of Allergy and Infectious Diseases, NIH).

Quantitative real-time PCR (RT-qPCR)

Total RNA was prepared with Trizol. First-strand cDNAs were synthesized with the QuantiTect Reverse Transcription Kit (Qiagen). Real-time PCR was performed using the QuantiTect SYBR Green PCR Kit (Qiagen) and normalized to β-actin (*Actb*) (primers are listed in supplementary material Table S1). Real-time PCR results are from three independent experiments with reactions performed in triplicate. Student's *t*-test was applied for statistical analysis ($P<0.05$).

Chromatin immunoprecipitation (ChIP)-PCR

The *in vivo* biotinylation ChIP assay was carried out as described previously (Kim et al., 2009). Briefly, ~20 E12.5 hearts with *Tbx20* homozygous biotin tag alleles ($Tbx20^{V5\text{-}Avi/V5\text{-}Avi}$;$Rosa26^{BirA/BirA}$) were isolated in ice-cold PBS and cross-linked with 1% formaldehyde for 10 minutes at room temperature. Extracted chromatin was sheared to ~100-500 bp, and then incubated with Dynabeads MyOne Streptavidin T1 beads (Invitrogen) at 4°C overnight. The magnetic beads were sequentially washed with 2% SDS, high salt buffer, LiCl buffer and TE buffer (He and Pu, 2010) before reversing the cross-linking at 65°C in elution buffer (10 mM Tris-HCl pH 8.0, 1 mM EDTA, 1% SDS) overnight. The immunoprecipitated DNA was then treated with proteinase K and purified using the MinElute PCR Purification Kit (Qiagen). Purified DNA was used as template for PCR. ChIP-PCR primers are listed in supplementary material Table S1.

Luciferase reporter assay

Mouse primary endocardial cell cultures from E11.5 hearts (Zhou et al., 2005) were grown in endothelial cell growth medium (EGM-2MV BulletKit, Lonza) with 10% fetal bovine serum. Cells were seeded in 1% gelatin-precoated 24-well plates until 85-95% confluent. These cells were transfected with a mixture of 200 ng luciferase reporter plasmid containing *Lef1* promoter fragments [or blank pGL3-TK vector (Promega) as control], 400 ng Tbx20 expression vector and 5 ng Renilla plasmid (pRL-TK as internal control) using X-tremeGENE 9 DNA Transfection Reagent (Roche) in Opti-MEM (Gibco) according to the manufacturer's instructions. After 48 hours of incubation, cells were lysed and assayed using the Dual-Luciferase Reporter Assay System (Promega). Luciferase/Renilla activity was quantified with the GloMax-Multi Detection System Kit (Promega). Genomic DNA fragments upstream of *Lef1* exon 1 were amplified by high-fidelity PCR and cloned into pGL3-TK (Fig. 6R). Primers used to generate the 3.9, 2.9 and 1.7 kb *Lef1* promoter fragments are listed in supplementary material Table S1. Results are from one representative experiment carried out in triplicate. At least three independent transfection experiments were performed.

RESULTS

Tbx20 is highly expressed in endocardial cushions and valve leaflets throughout mouse heart formation

Tbx20 is expressed in myocardial and endocardial cells during mouse cardiogenesis (Stennard et al., 2005; Takeuchi et al., 2005). To fully characterize *Tbx20* expression and its potential roles in heart formation, we generated a $Tbx20^{nlacZ/H2BGFP}$ knock-in mouse by inserting a *LoxP-nlacZ-polyA-LoxP-H2BGFP-polyA* cassette into the *Tbx20* start codon (with minimal deletion of exon 1 coding sequence). The expression of *nlacZ/H2BGFP* is driven by *Tbx20* endogenous regulatory elements (supplementary material Fig. S1), and *H2BGFP* expression is blocked when the *nlacZ* (nuclear *lacZ*) cassette is present. Whole-mount X-Gal staining showed that $Tbx20^{nlacZ}$ faithfully recapitulates *Tbx20* mRNA expression in the heart throughout embryogenesis (Fig. 1A,B; supplementary material Fig. S2). The $Tbx20^{H2BGFP}$ allele was generated by crossing $Tbx20^{nlacZ/H2BGFP}$ to *Protamine-Cre* mice (O'Gorman et al., 1997). With $Tbx20^{H2BGFP}$, we detected co-expression of *Tbx20* and *Nfatc1*, a marker of early endocardial cells (including cushion endocardial cells) (de la Pompa et al., 1998; Ranger et al., 1998) (Fig. 1C-F). From mid to late gestation, *Tbx20* expression continues in the cushion mesenchyme (Fig. 1G-J) and the leaflets of all four cardiac valves (Fig. 1K-N). *Tbx20* expression is maintained at high levels in the valve leaflets postnatally and into adulthood (Fig. 1O-R). The prominent expression of *Tbx20* in endocardial cushions and valve leaflets suggests a potential role in their development.

Disruption of *Tbx20* in endocardium results in embryonic lethality and defective valve formation and function

To investigate the role of *Tbx20* in endocardial cushion and valve morphogenesis, we crossed $Tbx20^{f/f}$ mice to $Nfatc1^{Cre/+}$;$Tbx20^{+/-}$ mice. During early cardiogenesis, *Nfatc1* is expressed throughout the endocardium from E9.5-10.5; at ~E11, *Nfatc1* expression becomes restricted to cushion endocardium (Chang et al., 2004). Lineage tracing analysis of $Nfatc1^{Cre/+}$ with $R26R^{lacZ}$ indicator mice revealed that $Nfatc1^{Cre/+}$ promotes recombination in the cushion endocardium and its mesenchymal derivatives (supplementary material Fig. S3) (Wu et al., 2012). Therefore, *Tbx20* is eliminated in both cushion endocardium and mesenchyme in $Nfatc1^{Cre/+}$;$Tbx20^{f/-}$ mice.

Mice with heterozygous deletion of *Tbx20* ($Nfatc1^{Cre/+}$;$Tbx20^{f/+}$ and $Nfatc1^{Cre/+}$;$Tbx20^{+/-}$) were viable and normal, yet the mutants [$Nfatc1^{Cre/+}$;$Tbx20^{f/-}$, *Tbx20* conditional knockout (CKO)] died between E14.5 and E16.5 (Fig. 2A). At E15.5, most mutant embryos had peripheral hemorrhage (Fig. 2B,C). Given that *Tbx20* and $Nfatc1^{Cre/+}$ only colocalize in the developing heart, we suspected cardiac dysfunction and failure as the cause of the lethality and hemorrhages. Histological analysis revealed that the valve leaflets in the mutants were shorter and blunt compared with those of littermate controls; all four valves were similarly affected at E14.5 (Fig. 2D-I).

To assess the effect of the dysmorphic valves on cardiac function, Doppler *in utero* echocardiography was performed on E14.5 embryos. As shown in Fig. 2J, waves above the baseline in control embryos represent normal transvalvular flow from the left ventricle to aorta across the aortic valve during systole. *Tbx20* CKO hearts had significant regurgitant flow (arrow in Fig. 2K). These initial observations demonstrate that endocardial *Tbx20* is essential for normal valve formation and function.

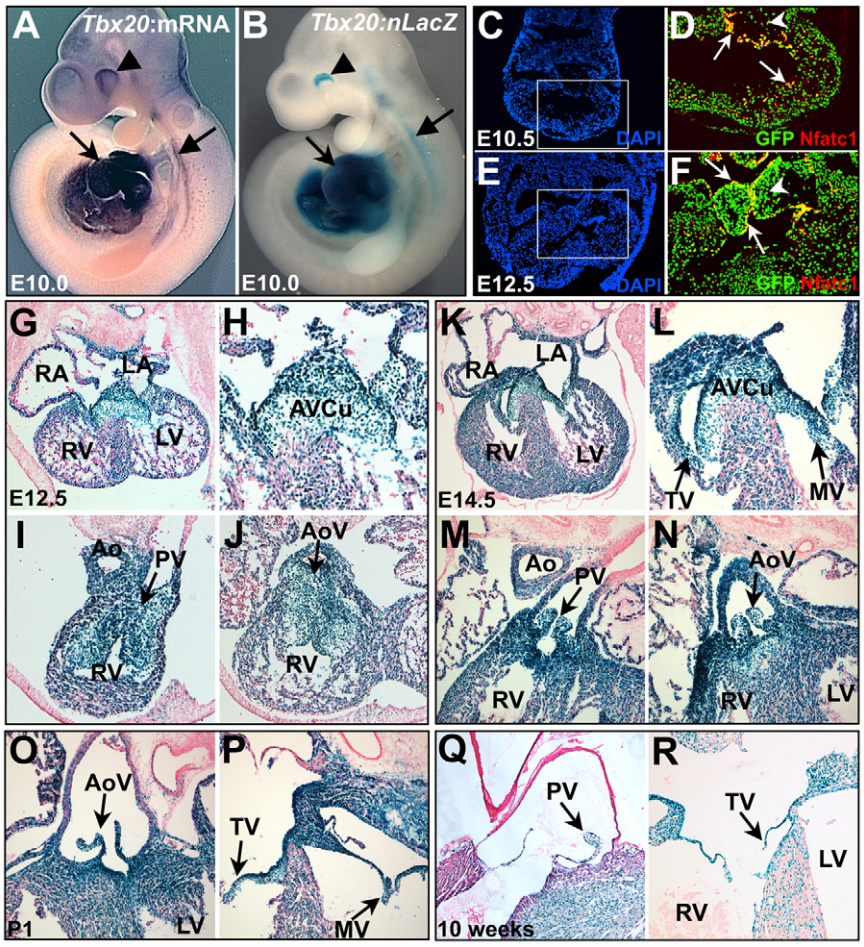

Fig. 1. Dynamic *Tbx20* expression in endocardial cushions and valves during mouse heart development. (**A**) Whole-mount RNA *in situ* hybridization to assess *Tbx20* expression in E10.0 mouse embryos. (**B**) X-Gal staining of a $Tbx20^{nlacZ}$ embryo faithfully recapitulates endogenous *Tbx20* expression in the heart (left arrow), neural tube (right arrow) and optic vesicle (arrowhead). (**C-F**) GFP from $Tbx20^{H2BGFP}$ and Nfatc1 immunostaining in the endocardium at multiple stages (arrows in D,F). *Tbx20* expression in cushion mesenchymal cells (arrowheads in D,F). The boxed regions in C and E are shown at higher magnification in D and F. (**G-N**) X-Gal staining of E12.5 and E14.5 cryosectioned $Tbx20^{nlacZ}$ hearts. $Tbx20^{nlacZ}$ is present in the endocardial cushions (H, arrows in I,J) and valve leaflets (arrows in L-N). H and L are higher magnification images of the atrioventricular cushion region from G and K. (**O-R**) $Tbx20^{nlacZ}$ is present in the remodeled valve leaflets from neonatal stages through adulthood (arrows). P1, postnatal day 1. Ao, aorta; AVCu, atrioventricular cushion; PV, pulmonary valve; AoV, aortic valve; RA/LA, right/left atrium; RV/LV, right/left ventricle; TV, tricuspid valve; MV, mitral valve.

Cushion and valve endocardial cells are less proliferative in *Tbx20* CKO embryos

Valve leaflets are formed by the elongation and thinning of valve primordia in a precisely controlled manner that is crucial for proper cardiac function (Hinton and Yutzey, 2011). To further characterize the valve defects in *Tbx20* CKO embryos, we examined the relative length of the valve leaflets at E14.5. The distance between the valve cusp and cushion base was set as the valve length (Stankunas et al., 2010). Disruption of *Tbx20* engendered much shorter and wider semilunar (pulmonary and aortic) valve leaflets (Fig. 3A-D), which were 66% and 69% of the length of the controls, respectively (Fig. 3G). Defective elongation of the mutant mitral and tricuspid valves was much more severe than that of the semilunar valves, both by histological examination (Fig. 3E,F) and by calculated relative valve length (Fig. 3G; 28% and 26% of control, respectively).

Cardiac valve elongation and remodeling start at E12.5 in mice and are characterized by rapid cell proliferation at the edge of the valve and apoptosis at the base of the cushion (Lin et al., 2012). The cardiac valve elongation defects in *Tbx20* CKO mice suggested deficient cell proliferation and/or survival, so we assessed proliferation and apoptosis in E13.5 hearts. Co-immunostaining for CD31 (Pecam1 – Mouse Genome Informatics) was used to identify endocardial cells. Representative results for the mitral valve are shown in Fig. 3H,I. We categorized and counted endocardial cells based on their location (endocardium versus mesenchyme). Interestingly, mutant mitral valve endocardial cells were much less proliferative (18% in mutant versus 32% in control), whereas mesenchymal cell proliferation was unchanged (32% in mutant versus 28% in control; Fig. 3L). Similar observations were made for the pulmonary, aortic and tricuspid valves (Fig. 3L). In addition, we detected very few apoptotic cells in the cushions of controls and mutants (Fig. 3J,K). These observations indicate that decreased proliferation of endocardial cells contributes to the valve elongation defects of *Tbx20* CKO embryos.

To determine the onset of the *Tbx20* CKO valve defects, we inspected endocardial cushion formation in E12.5 embryos. AVC and OFT cushions were measured and relative cushion sizes were calculated (Jiao et al., 2006). The pulmonary and aortic valves were properly formed in the mutants with little or no change in cushion size at this stage (98% and 97% of control, respectively; Fig. 4A-D,I), whereas the AV cushions were smaller than in controls (64% of control; Fig. 4E-I). At E11.5, AV cushion size and morphology were indistinguishable from controls (supplementary material Fig. S4), as was cushion mesenchymal cell proliferation (28% in mutant and 26% in control; Fig. 4J-M,P). However, there were fewer proliferating cushion endocardial cells in mutant hearts (24% in mutant versus 35% in control; Fig. 4J-M,P). Very few apoptotic cells were detected in mutant or control AVC cushions at E11.5 (Fig. 4N,O). These observations indicate that the abnormal proliferation of the valve endocardial cells begins at E11.5 and disrupts atrioventricular cushion formation.

Endocardial *Tbx20* is not required for EMT in AVC and OFT development

During early embryogenesis (~E7.5-8.0 in mice), the earliest endocardial cells derive from endothelium within the heart tube

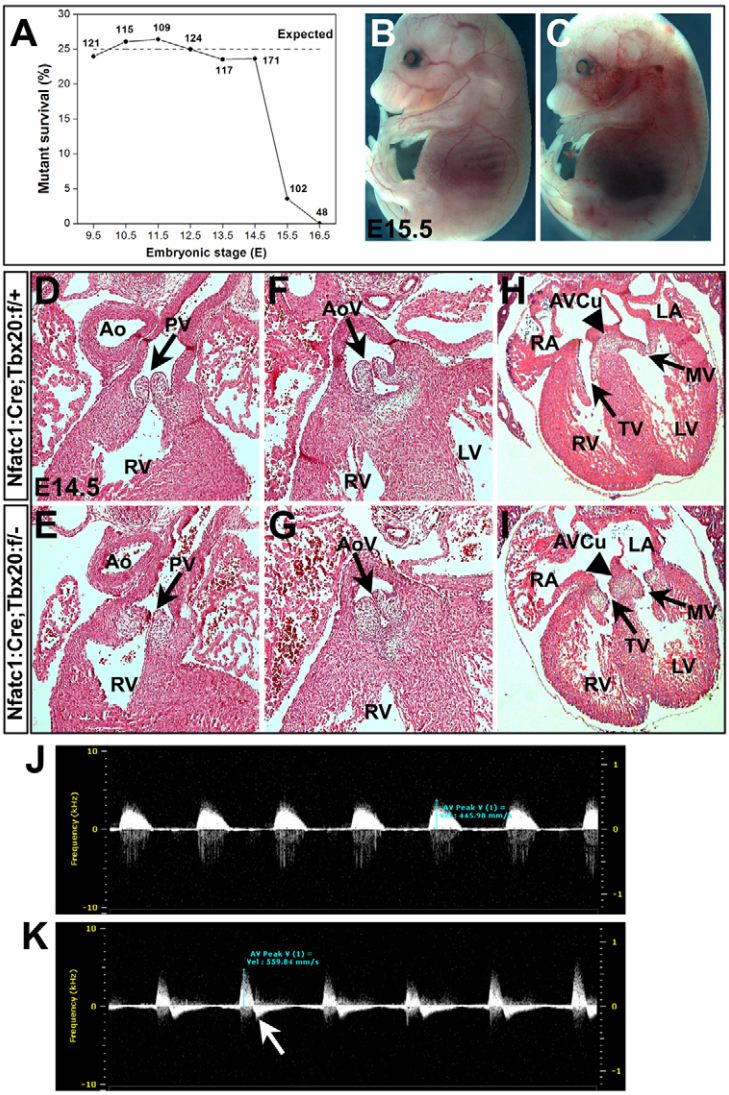

Fig. 2. *Tbx20* endocardial deletion causes embryonic lethality with cushion and valve developmental defects. (**A**) *Tbx20* CKO embryos die by E16.5. Incidence of *Tbx20* CKO embryos at each embryonic stage and the expected survival percentage (25%, dashed line). Numbers indicate total embryos genotyped. (**B**,**C**) *Tbx20* CKO embryos exhibit peripheral hemorrhage over the body at E15.5. (**D-I**) Transverse sections of *Tbx20* CKO mutant (E,G,I) and control (D,F,H) hearts at E14.5. The mutant valves, including the pulmonary valve (arrows in D,E), aortic valve (arrows in F,G), tricuspid valve and mitral valve (arrows in H,I), are shorter and blunt relative to those of controls. (**J**,**K**) Doppler *in utero* echocardiography. In the E14.5 control embryos (J), the waves above the baseline represent normal systolic transvalvular flow from left ventricle to aorta during systole. *Tbx20* CKO mutant hearts (K) show regurgitant flow (arrow) across the aortic valve, which is indicative of valve incompetence.

(Armstrong and Bischoff, 2004). After this transition, endocardial cells give rise to the cushion mesenchyme in the AVC and OFT through EMT (~E9.5-10.5 in mice). Previous studies suggest that perturbed EMT results in abnormal valve formation (Person et al., 2005). Based on this, we examined whether EMT initiation is disrupted by *Tbx20* endothelial loss of function. We introduced the *R26R*^{lacZ} allele (Soriano, 1999) into the genetic crosses to trace endocardial-derived cells in the mesenchyme. No significant difference was observed in the number of cushion mesenchymal cells in mutants and controls at E10.5 (supplementary material Fig. S5A-D). It is important to note that endocardial-derived mesenchymal cells are located in the proximal OFT [pOFT; positive for X-Gal staining (X-Gal^{+})], whereas cardiac neural crest-derived mesenchymal cells are located in distal OFT (dOFT, X-Gal^{-}) (Lin et al., 2012; Park et al., 2008; Wu et al., 2011). Furthermore, we did not detect any differences in the number of X-Gal^{+} mesenchymal cells in the AVC and OFT at this stage (supplementary material Fig. S5E). We examined the expression of several genes important for EMT at E9.5-10.5, including *Bmp2* and *Tgfb2* in the AVC and OFT myocardium (Ma et al., 2005; Person et al., 2005) and *Sox9* and *Snail1* in cushion mesenchyme (Akiyama et al., 2004; Timmerman et al., 2004). RNA *in situ* hybridization showed that the expression of these genes was normal (supplementary material Fig. S5F-U).

To ensure that the unaffected EMT was not the result of inefficient deletion of *Tbx20* in the endocardium, we examined Tbx20 protein by immunostaining and *Tbx20* exon 2 RNA by *in situ* hybridization in the hearts (exon 2 was flanked by *LoxP* sites in *Tbx20* floxed mice) (Cai et al., 2005). This confirmed complete ablation of Tbx20 in the AVC endocardial and mesenchymal cells of *Tbx20* CKO hearts at E9.25, just prior to EMT initiation (supplementary material Fig. S6). The expression of other genes crucial for endocardial cushion and valve development, including *Bmp4* (Jiao et al., 2003), *Notch1* (Timmerman et al., 2004), *Gata4* (Rivera-Feliciano et al., 2006), *Tbx5* (Nadeau et al., 2010) and *Nfatc1* (de la Pompa et al., 1998; Ranger et al., 1998) was unchanged in *Tbx20* CKO hearts (supplementary material Figs S7, S8). These results suggest that endocardial *Tbx20* is not essential for EMT initiation in the AVC or OFT.

Disturbed Wnt/β-catenin signaling in *Tbx20* CKO hearts

To identify molecular mechanisms underlying the endocardial cushion and valve defects in *Tbx20* CKO hearts, we applied high-throughput mRNA sequencing (mRNA-Seq) to identify differentially expressed genes in mutants versus controls. We chose E12.5 hearts for analysis because valve elongation and remodeling

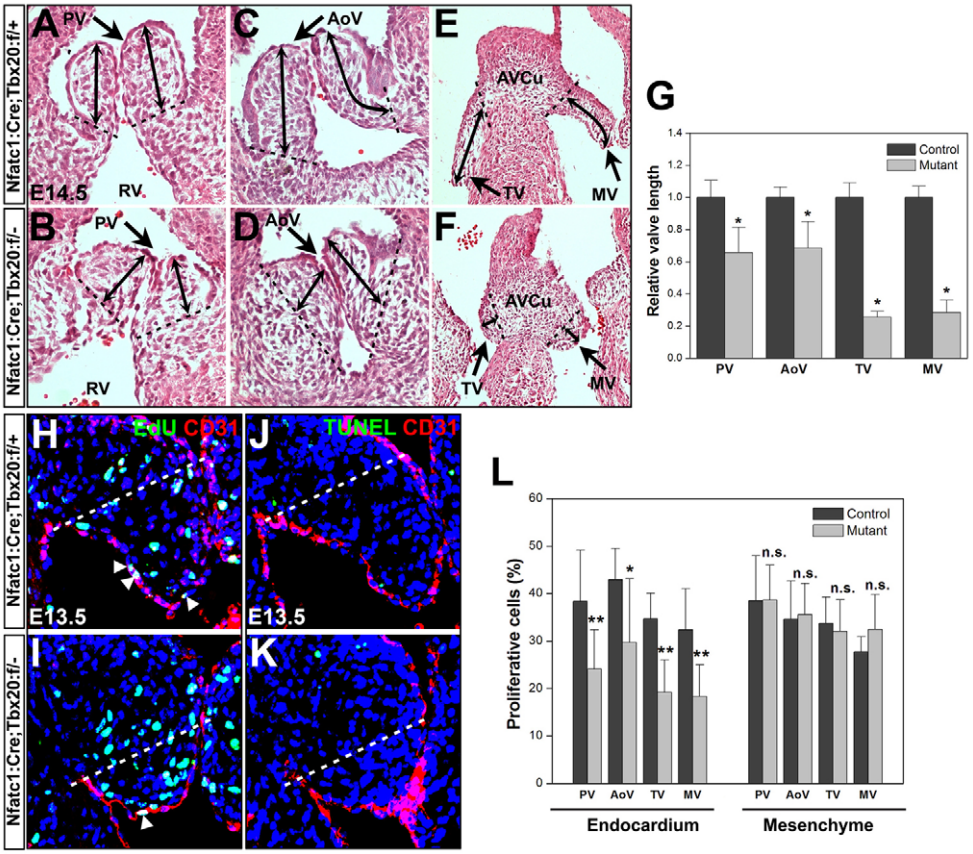

Fig. 3. *Tbx20* endocardial deletion disrupts valve elongation and endocardial cell proliferation. (**A-F**) *Tbx20* CKO mutant and control valves at E14.5. Arrows indicate pulmonary valve (A,B), aortic valve (C,D), tricuspid valve and mitral valves (E,F). Valve length is indicated by doubleheaded arrows. Dashed lines mark the junctions between valve base and cusp. (**G**) Relative valve length. (**H**,**I**) Proliferating cells in mitral valves detected by EdU staining (green) at E13.5. CD31 co-staining (red) marks valve endocardial cells. Arrowheads indicate proliferating endocardial cells. (**J**,**K**) Apoptotic cells (green) detected by TUNEL in control and mutant mitral valves at E13.5. Dashed lines in H-K indicate the junction between valve base and cusp. (**L**) Statistical comparison of valve endocardial and mesenchymal cell proliferation at E13.5. Decreased cell proliferation is observed in the valve endocardium but not the mesenchyme. *P<0.05, **P<0.01, versus control. n.s., not significant. Error bars indicate s.d.

begin at this stage in mice (Wirrig and Yutzey, 2011) and *Tbx20* CKO valve defects are first evident (Fig. 4A-H). mRNA-Seq assays were carried out on three pooled mutant hearts with corresponding littermate controls. More than 30 million raw reads were generated per sample. Among these, more than 20 million reads were uniquely mapped to mouse RefSeq transcripts using BWA alignment.

A total of 112 differentially expressed genes were identified with at least a 1.5-fold change between the mutant and control (supplementary material Table S2). Ingenuity pathway analysis (Fig. 5A; supplementary material Table S3) as well as Gene Ontology enrichment analysis (Fig. 5B; supplementary material Table S4) identified Wnt/β-catenin pathway genes, including *Wnt7b*, *Wnt9b* and *Lef1*, among the significantly dysregulated genes (Fig. 5C). This bioinformatic result was validated by RT-qPCR on E10.5-12.5 hearts, and we detected changes in the expression of these genes as early as E11.5 (Fig. 5D), prior to the appearance of *Tbx20* CKO cushion developmental defects (Fig. 4A-H; supplementary material Fig. S4). In addition, when we further assessed the expression of Wnt pathway genes in the developing cushion and valve cells by RNA *in situ* hybridization, we found that *Wnt4* and *Wnt9b* expression in cushion endocardium (Alfieri et al., 2010) was decreased in the mitral and pulmonary valves of *Tbx20* CKO mutants (Fig. 6A-H, Fig. 5D). Given the altered expression of these Wnt ligand genes, we then examined the expression of Tcf/Lef transcription factors [*Lef1* and *Tcf1* (*Tcf7* – Mouse Genome Informatics), *Tcf3* and *Tcf4*] in the heart, and found that only *Lef1* was expressed in the cushion endocardium and adjacent cells (Fig. 6I,K,M,O; supplementary material Fig. S9; data not shown for *Tcf1/3/4*). Intriguingly, *Lef1* was notably decreased in the cushion endocardium of the mutant mitral and pulmonary valves (Fig. 6J,L,N,P,Q). *Fzd2* (Alfieri et al., 2010) expression was unchanged in the atrioventricular cushions (data not shown). These results reveal that Tbx20 is required for the normal expression of Wnt/β-catenin pathway genes during cardiac valve formation.

To determine whether the changed expression of these genes correlated with altered Wnt/β-catenin signaling in the *Tbx20* CKO hearts, we introduced the *TOPGAL* indicator allele into the genetic crosses (DasGupta and Fuchs, 1999). At E10.5-12.5, whole-mount X-Gal staining of the *TOPGAL* embryos revealed increasing Wnt/β-catenin signaling activity in the endocardial cushion regions, and later in all four developing valves (supplementary material Fig. S10). Signaling was greatest in the growing edge of the atrioventricular valves, including the endocardium and subadjacent mesenchymal cells (Fig. 5E,G,I,K). Interestingly, we found that *lacZ*-expressing cells were dramatically decreased in the mutant atrioventricular valves (Fig. 5F,H,J,L), consistent with reduced Wnt/β-catenin signaling in *Tbx20* CKO hearts at E11.5-12.5 (Fig. 5D, Fig. 6A-Q). The reduced *lacZ* expression was confirmed by RT-qPCR (Fig. 5M).

Given the central role of Tcf/Lef transcription factors in mediating Wnt/β-catenin signaling, we questioned whether downregulation of *Lef1* in *Tbx20* CKO cushion endocardial cells was the result of direct regulation by Tbx20 as opposed to loss of Wnt/β-catenin signaling. We aligned orthologous genomic sequences flanking *Lef1* in mouse, rat and human and found a conserved putative T-box binding site upstream of exon 1 (Fig. 6R,S). ChIP on E12.5 hearts isolated from doubly homozygous *Tbx20* biotin tag knock-in mice ($Tbx20^{V5\text{-}Avi/V5\text{-}Avi}$;$Rosa26^{BirA/BirA}$; Fig. 6T; see Materials and methods) (Driegen et al., 2005) revealed that Tbx20 bound to this location (Fig. 6U, P1+P2), but not to a nearby control region (Fig. 6U, P3+P4). Cardiac tissues collected from $Rosa26^{BirA/BirA}$ control mice (without $Tbx20^{V5\text{-}Avi}$ alleles)

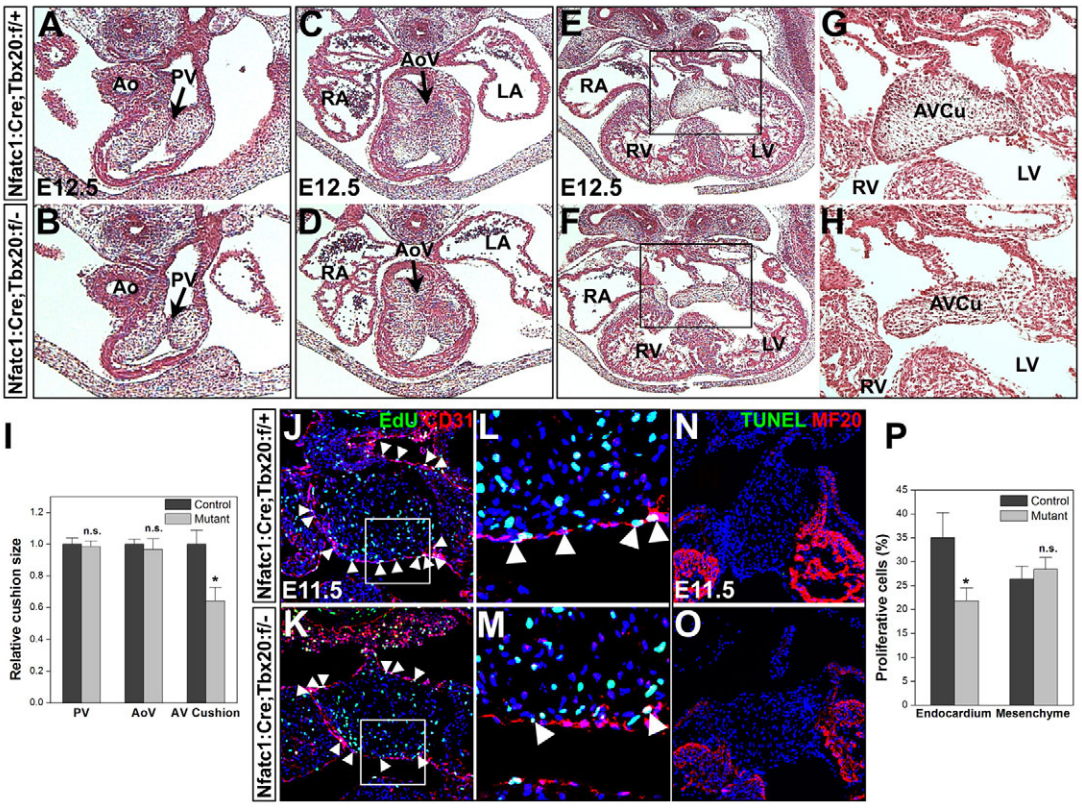

Fig. 4. Defective atrioventricular cushion formation in *Tbx20* CKO embryos. (**A-H**) Transverse sections of *Tbx20* CKO mutant and control hearts at E12.5. Arrows indicate endocardial cushions in the pulmonary valve (A,B) and aortic valve (C,D). G and H are higher magnification images of the atrioventricular cushion region (boxed) from E and F. (**I**) Relative cushion size was determined for pulmonary valve, aortic valve and atrioventricular cushion. The mutant atrioventricular cushions are smaller than in the control, whereas the pulmonary valve and aortic valves are normal in size at E12.5. (**J-M**) Proliferative cells are labeled by EdU staining (green) in the atrioventricular cushions at E11.5. CD31 co-staining (red) labels cushion endocardial cells. Arrowheads indicate proliferating endocardial cells. L and M are higher magnification images of the atrioventricular cushion region (boxed) from J and K. (**N**,**O**) Few apoptotic cells (green) are found in the atrioventricular cushion region of mutant and control embryos. MF20 antibody (red) labels myocardial cells. (**P**) At E11.5, mutant atrioventricular cushion endocardial cell proliferation is significantly slower than in the control, whereas mesenchymal cell proliferation is relatively normal. **P*<0.05, versus control. n.s., not significant. Error bars indicate s.d.

showed no recruitment of Tbx20 (Fig. 6U, lane 3). Further, luciferase reporter assays with mouse embryonic endocardial cell cultures (Zhou et al., 2005) revealed activation of the *Lef1* promoter by Tbx20 in the fragment containing the Tbx20 binding site (3.9 kb) but not in fragments without this site or that were negative in ChIP-PCR (2.9 kb and 1.7 kb) (Fig. 6R,U,V).

Combined with the aforementioned expression data, these results suggest that direct binding of Tbx20 to the *Lef1* promoter regulates *Lef1* expression in the cushion endocardium during cardiac valve formation. In addition, we scanned the *Wnt4* and *Wnt9b* promoters (~3 kb upstream of the transcriptional start site) by ChIP-PCR to determine whether Tbx20 also binds to the regulatory elements of these genes, but no enriched elements were detected (data not shown).

Disrupted ECM integrity in *Tbx20* CKO endocardial cushion

Endocardial cushion ECM composition is crucial for mesenchymal cell migration, proliferation and differentiation (Hinton et al., 2006), and subsequent valve leaflet formation is also inextricably linked to ECM remodeling (Chakraborty et al., 2010; Hinton and Yutzey, 2011). Thus, we further examined the transcription of ECM components in *Tbx20* CKO hearts by RT-qPCR. *Postn* is essential for ECM integrity and is required for valve remodeling and maturation (Snider et al., 2008). We found that *Postn* was downregulated in *Tbx20* CKO hearts (Fig. 7A). RNA *in situ* hybridization confirmed that downregulation of *Postn* was localized to the cushion cells (Fig. 7B-E). Matrix metalloproteinases (MMPs) are secreted extracellular proteases essential for the degradation and remodeling of ECM components in the valve (Shelton and Yutzey, 2007). *Mmp13* expression was decreased in the cushion of *Tbx20* CKO hearts, whereas expression of *Mmp2* and *Mmp9* was not (Fig. 7A,F,G). Chondroitin sulfate proteoglycans and collagens are important ECM components. RT-qPCR and immunostaining revealed downregulated *Acan* expression in *Tbx20* CKO hearts (Fig. 7A,H,I). Hyaluronic acid (HA) synthase 2 (Has2) is crucial for ECM organization (Camenisch et al., 2000). *Has2* expression was normal in mutant hearts (Fig. 7A), consistent with Alcian Blue staining showing a normal distribution of HA in the ECM (Fig. 7J-M). The altered expression of *Postn*, *Mmp13* and *Acan* could affect ECM integrity in the cushion, which might further aggravate the proliferation and valve elongation deficiency of *Tbx20* CKO hearts.

DISCUSSION

T-box transcription factors play fundamental roles in development and disease (Greulich et al., 2011). Ablation of *Tbx1*, *Tbx2*, *Tbx3*,

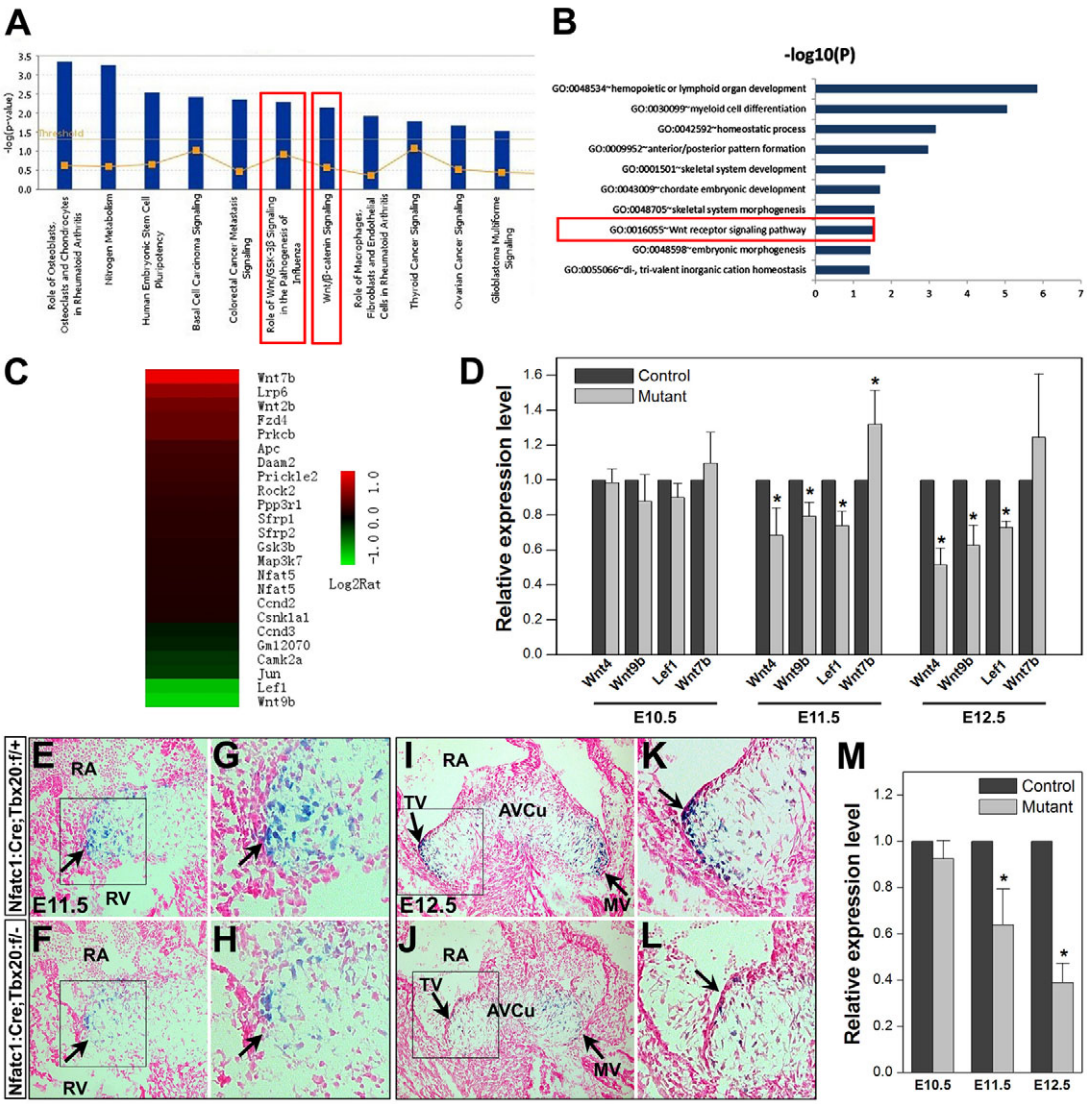

Fig. 5. *Tbx20* loss of function in endocardium disrupts Wnt/β-catenin signaling in developing valves. (**A**) Significant canonical pathways identified from genes differentially expressed in *Tbx20* CKO versus control by ingenuity pathway analysis. The *y*-axis is the $-\log_{10}$ of the *P*-value for the enrichment of a pathway in the input gene list compared with genes in the whole genome. Red boxes highlight Wnt/β-catenin signaling pathway. The zigzag orange line indicates the enrichment ratio of the percentage of genes in a particular pathway over the percentage of pathway genes in the genome. (**B**) Significant Gene Ontology (GO) terms identified in the differentially expressed genes. *x*-axis is the $-\log_{10}$ of the *P*-value for the enrichment of a GO term in the input gene list compared with genes in the whole genome. (**C**) Heat map of Wnt signaling pathway genes. Red and green denotes upregulated and downregulated genes, respectively, in the *Tbx20* CKO. (**D**) Relative expression of Wnt pathway genes at E10.5-12.5 determined by RT-qPCR. (**E-L**) X-Gal staining of *TOPGAL* indicator mice to detect active Wnt/β-catenin signaling at E11.5 (E-H) and E12.5 (I-L). The mutant tricuspid and mitral valves display fewer X-Gal-stained cells and fainter staining in the positive cells in both endocardium and adjacent mesenchyme (arrows in F,H,J,L versus E,G,I,K). G,H and K,L are higher magnification images of the tricuspid valve region (boxed) from E,F and I,J. (**M**) Relative expression of *lacZ* at different stages as determined by RT-qPCR. **P*<0.05, versus control. Error bars indicate s.d.

Tbx5 or *Tbx20* in mice leads to cardiac malformations (Naiche et al., 2005). Human *TBX1* mutations play a major role in 22q11 deletion syndrome, which includes serious cardiac defects (Merscher et al., 2001). *TBX5* mutations cause Holt-Oram syndrome with atrial and ventricular septal defects (ASD and VSD) (Basson et al., 1997). Human *TBX20* mutations are associated with a complex spectrum of cardiac developmental and functional abnormalities including total anomalous pulmonary venous connection (TAPVC), ASD (Liu et al., 2008; Posch et al., 2010), VSD (Qiao et al., 2012), tetralogy of Fallot (TOF) (Liu et al., 2008) and cardiomyopathies with defective valvulogenesis (Kirk et al., 2007; Qian et al., 2008). In the present study we eliminated *Tbx20* in the endocardium of mouse embryos and provide the first genetic evidence that *Tbx20* is crucial for endocardial cushion maturation and valve elongation in mammals. Our data suggest that decreased proliferation of valve endocardial cells contributes to the valve elongation defects in *Tbx20* CKO hearts. These findings advance our understanding of the developmental and pathological processes leading to human congenital valve defects associated with *TBX20* mutations.

Previous studies showed that Tbx20 regulates endocardial cushion mesenchymal cell proliferation in avian cushion explants

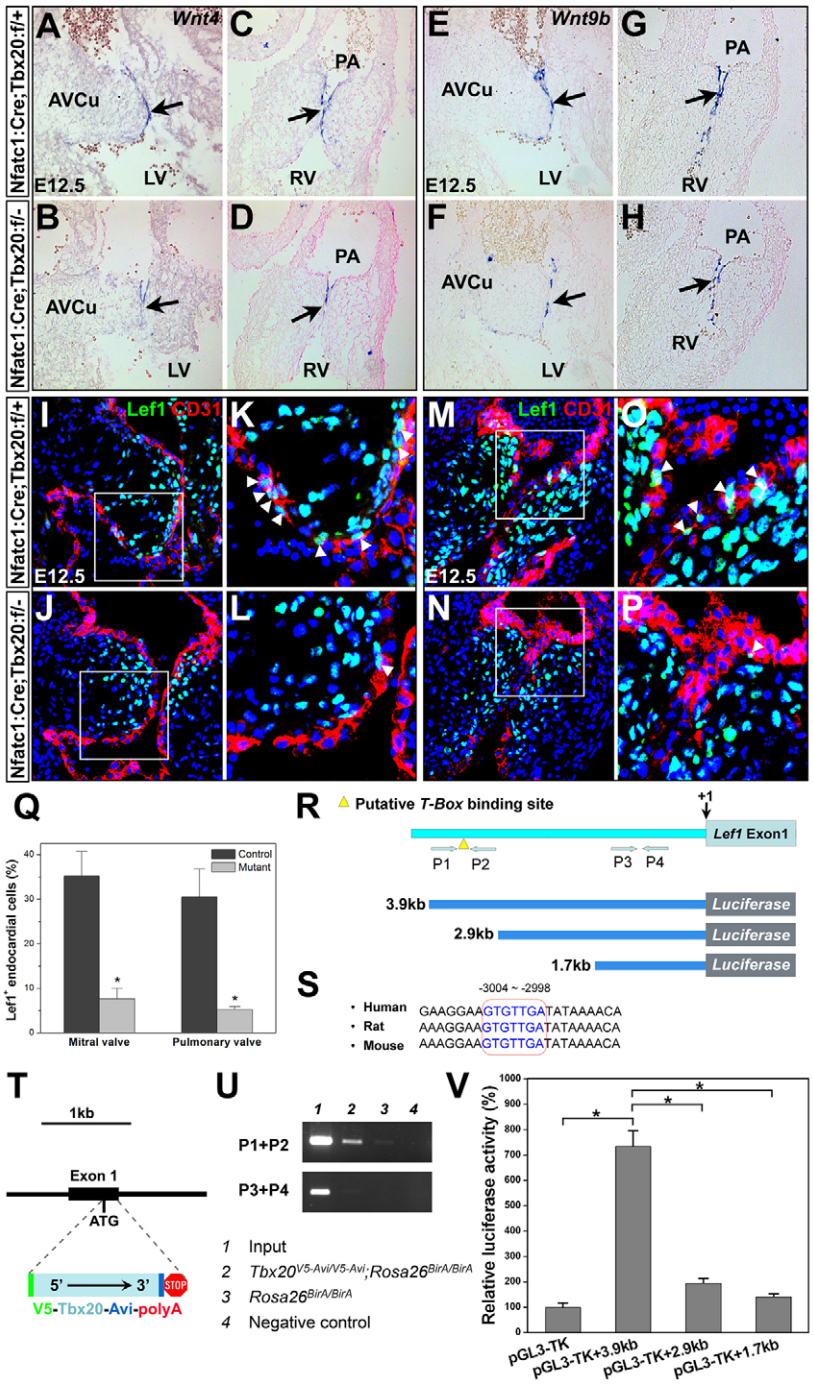

Fig. 6. Misexpression of Wnt/β-catenin pathway genes in the valve endocardium of *Tbx20* CKO hearts. (**A-H**) RNA *in situ* hybridization of *Wnt4* and *Wnt9b* in the mitral (A,B,E,F) and pulmonary (C,D,G,H) valve endocardial cells in control (A,C,E,G) and *Tbx20* CKO mutant (B,D,F,H). Arrows indicate valve endocardial cells. (**I-P**) Downregulated Lef1 (green) expression in mitral (I-L) and pulmonary (M-P) valve endocardial cells in the mutants (arrowheads in K,L,O,P). CD31 (red) co-staining marks endocardium. K,L and O,P are higher magnification images of the boxed regions from I,J and M,N. Nuclei are labeled by DAPI (blue). (**Q**) Comparison of the number of Lef1$^+$ endocardial cells in mitral and pulmonary valves in control and mutant hearts at E12.5. *P<0.05, versus control. (**R**) The putative T-box binding site in the *Lef1* promoter and luciferase reporter constructs containing 3.9 kb, 2.9 kb and 1.7 kb *Lef1* promoter fragments (in the pGL3-TK vector). P1-P4 refer to the ChIP-PCR primers. (**S**) Alignment of *Lef1* genomic sequences in human, rat and mouse. The putative T-box binding site is highlighted (red circle). (**T**) In *Tbx20*$^{V5\text{-}Avi}$ biotin tag knock-in mice, full-length *Tbx20* cDNA is fused with *V5* and *Avi* (*V5-Tbx20-Avi-polyA*) and the cassette is inserted into the start codon of the *Tbx20* genomic locus. (**U**) ChIP-PCR on E12.5 heart tissues (from *Tbx20*$^{V5\text{-}Avi/V5\text{-}Avi}$;*Rosa26*$^{BirA/BirA}$ doubly homozygous mice) using the primers shown in R demonstrates recruitment of Tbx20 to regions containing the T-box consensus site within the *Lef1* promoter (P1+P2); ChIP-PCR with primers against a different region reveals no Tbx20 recruitment (P3+P4). No recruitment was found with heart tissues from *Rosa26*$^{BirA/BirA}$ mice (lane 3, control). Negative control, H_2O as PCR template. (**V**) Luciferase reporter assays of the Tbx20 expression vector with various *Lef1* promoter fragments. The 3.9 kb fragment containing the putative T-box binding site activates the luciferase reporter significantly, whereas the 2.9 kb and 1.7 kb fragments without the binding site do not. *P<0.01, paired *t*-test. Error bars indicate s.d. PA, pulmonary artery.

(Shelton and Yutzey, 2007). In our analysis of *Nfatc1*$^{Cre/+}$;*Tbx20*$^{f/-}$ mice, we detected lower proliferation in the valve endocardium but not cushion mesenchyme. The ECM gene *Mmp13* was downregulated (as seen in chicken cushion cell cultures), whereas *Mmp9* was not (in contrast to in chicken cushion cell cultures) (Shelton and Yutzey, 2007). These discrepancies might reflect divergent regulation of this developmental process in different species or the different experimental approaches used.

During mouse embryogenesis, several Wnt/β-catenin pathway genes are specifically expressed in the developing valves (Alfieri et al., 2010). A previous study of β-catenin endocardial deletion mice showed that Wnt/β-catenin signals play crucial roles in endocardial EMT, and mutant mice died at E11.5-13.0 with severe EMT abnormities (Liebner et al., 2004). Despite the specific expression of Wnt/β-catenin pathway genes in the developing valves (Alfieri et al., 2010), it is largely unknown whether Wnt/β-catenin signaling is required for valve elongation and remodeling at mid to late gestation. In the mRNA-Seq analysis of *Tbx20* CKO hearts, we found that the levels of transcripts encoding Wnt/β-catenin pathway genes were significantly changed (Fig. 5). Further analysis demonstrated that *Wnt4*, *Wnt9b* and *Lef1* were downregulated in valve endocardial cells (Fig. 6). Misexpression of *Wnt4* and *Wnt9b* in the cushion endocardial cells might affect β-catenin stabilization and translocation into the nucleus in *Tbx20* CKO hearts (van Amerongen and Nusse, 2009).

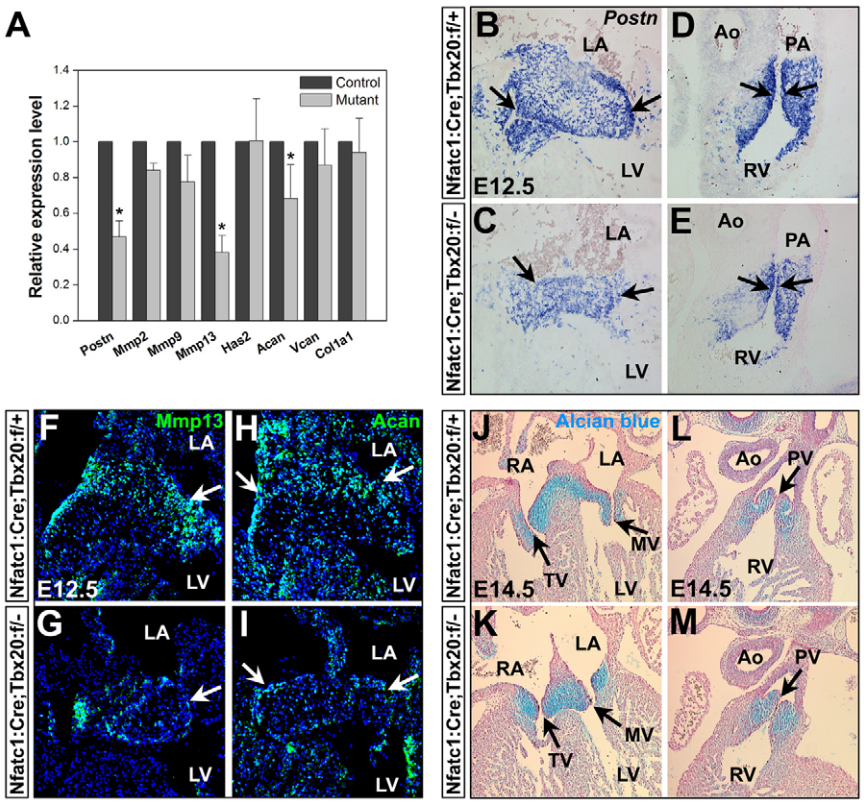

Fig. 7. Altered expression of ECM genes in *Tbx20* CKO heart. (**A**) Relative expression of ECM genes as determined by RT-qPCR on E12.5 hearts. *Postn*, *Mmp13* and *Acan* are significantly downregulated in the *Tbx20* CKO heart. **P*<0.05, versus control. Error bars indicate s.d. (**B-E**) RNA *in situ* hybridization of *Postn* expression in atrioventricular (B,C) and pulmonary (D,E) cushion endocardial and mesenchymal cells at E12.5. Arrows indicate cushion endocardial cells. (**F-I**) Immunostaining of Mmp13 (F,G) and Acan (H,I) in atrioventricular cushion at E12.5. Arrows indicate cushion endocardial cells. (**J-M**) Alcian Blue staining of hyaluronic acid in atrioventricular and pulmonary valves at E14.5.

Lef1 belongs to the Tcf/Lef transcription factor family, which bind DNA through a high mobility group domain (Cadigan and Waterman, 2012). In the absence of Wnts, Tcf/Lefs repress transcription in association with co-repressors such as Groucho. Nuclear accumulation of β-catenin in response to Wnt signaling drives Tcf/Lef regulation of Wnt-responsive gene expression (Clevers and Nusse, 2012). It is important to note that *Lef1*-deficient mice have morphogenetic defects in several organs that require epithelial-mesenchymal interactions (van Genderen et al., 1994), and Wnt/β-catenin signaling has been widely proven to be essential for organ growth during development (Clevers and Nusse, 2012; Gessert and Kühl, 2010; Wang et al., 2012; Zimmerman et al., 2012). Based on this, we postulate that aberrant Wnt/β-catenin signaling is a major contributor to the proliferative defects in *Tbx20* CKO cushions and valves. Additional studies are needed to determine whether there is an ongoing Tbx20→Wnt/β-catenin cascade needed for valve maturation and elongation during the fetal stages of mouse heart development.

Our ChIP-PCR assay with cardiac tissues revealed that Tbx20 directly binds the *Lef1* promoter (Fig. 6). It is important to note that, in *Tbx20* CKO hearts, *Tbx20* was disrupted in both the endocardium and its cushion mesenchyme derivatives. In *Tbx20* CKO hearts Lef1 expression was downregulated in the endocardium, whereas the expression in the cushion mesenchyme was relatively normal (Fig. 6), indicating that, at least in the cushion mesenchyme, Tbx20 is not required for *Lef1* expression. Therefore, regulation of *Lef1* by Tbx20 might be cell context dependent, and co-factors in different cell contexts at different developmental stages might play a crucial role in these transcriptional regulation processes. Moreover, Tbx20 is likely to bind regulatory elements in many other genes (in addition to *Lef1*) to systematically coordinate cushion development and valve elongation. Future genome-wide ChIP-Seq analysis will help to determine which of the 112 differentially expressed genes in *Tbx20* CKO hearts (>1.5-fold; supplementary material Table S2) are direct targets of Tbx20 and have important impacts on valve development.

It is noteworthy that the pulmonary and aortic valves in *Tbx20* CKO embryos exhibit less severe defects than the atrioventricular valves (Figs 3, 4). This might be due to the different developmental origins of the semilunar and atrioventricular valves. During mouse heart development, the OFT valves are derived from multiple lineages including endocardium, neural crest and second heart field (Jain et al., 2011; Lin et al., 2012), whereas the atrioventricular valves are almost entirely derived from endocardium (de Lange et al., 2004) and thus have the largest number of cells affected by $Nfatc1^{Cre/+}$-mediated genetic excision (Wu et al., 2012).

Taken together, our studies revealed a crucial role for Tbx20 in endocardial cushion formation and valve elongation in mice. The valve elongation defects of *Tbx20* CKO hearts are associated with fewer proliferative cushion endocardial cells, aberrant Wnt/β-catenin signaling and reduced ECM gene expression. Tbx20 directly regulates the key Wnt transcriptional effector *Lef1* through binding its promoter element. These studies provide genetic insight into the etiology of human congenital valve disease associated with *TBX20* mutations.

Acknowledgements
We thank Drs Bruce Gelb and Anne Moon for critical reading of the manuscript; Dr Katherine Yutzey (Cincinnati Children's Medical Center) for RNA *in situ* probes; and Drs Yong Zhao, Yusheng Wei, Michael Rendl at Mount Sinai and Drs Kai Mao and Yidong Wang at Albert Einstein College of Medicine for experimental support.

Funding
This work is supported by grants to C.L.C. from the National Institutes of Health (NIH)/National Heart, Lung, and Blood Institute (NHLBI) [1R01HL095810 and 1K02HL094688]; New York State Stem Cell Science (NYSTEM) [C026426];

the American Heart Association [0855808D]; and the March of Dimes Foundation [5-FY07-642]. B.W. is supported by a grant from the NIH/NHLBI [HL078881]. Deposited in PMC for release after 12 months.

Competing interests statement
The authors declare no competing financial interests.

Author contributions
X.C. conceived the project, designed and performed the experiments, and prepared the manuscript. W.Z. performed RNA-Seq data analysis. J.H., L.Z., N.S. and W.C. provided experimental assistance. B.W. and B.Z. contributed to the reagents and manuscript preparation. C.-L.C. conceived the project, designed the experiments, and prepared and approved the manuscript.

Supplementary material
Supplementary material available online at
http://dev.biologists.org/lookup/suppl/doi:10.1242/dev.092502/-/DC1

References
Akiyama, H., Chaboissier, M. C., Behringer, R. R., Rowitch, D. H., Schedl, A., Epstein, J. A. and de Crombrugghe, B. (2004). Essential role of Sox9 in the pathway that controls formation of cardiac valves and septa. *Proc. Natl. Acad. Sci. USA* **101**, 6502-6507.
Alfieri, C. M., Cheek, J., Chakraborty, S. and Yutzey, K. E. (2010). Wnt signaling in heart valve development and osteogenic gene induction. *Dev. Biol.* **338**, 127-135.
Armstrong, E. J. and Bischoff, J. (2004). Heart valve development: endothelial cell signaling and differentiation. *Circ. Res.* **95**, 459-470.
Bancroft, J. D. and Gamble, M. (2008). *Theory and Practice of Histological Techniques*. Philadelphia, PA: Churchill Livingstone Elsevier.
Basson, C. T., Bachinsky, D. R., Lin, R. C., Levi, T., Elkins, J. A., Soults, J., Grayzel, D., Kroumpouzou, E., Traill, T. A., Leblanc-Straceski, J. et al. (1997). Mutations in human TBX5 cause limb and cardiac malformation in Holt-Oram syndrome. *Nat. Genet.* **15**, 30-35.
Beppu, H., Malhotra, R., Beppu, Y., Lepore, J. J., Parmacek, M. S. and Bloch, K. D. (2009). BMP type II receptor regulates positioning of outflow tract and remodeling of atrioventricular cushion during cardiogenesis. *Dev. Biol.* **331**, 167-175.
Cadigan, K. M. and Waterman, M. L. (2012). TCF/LEFs and Wnt signaling in the nucleus. *Cold Spring Harb. Perspect. Biol.* **4**, a007906.
Cai, C. L., Zhou, W., Yang, L., Bu, L., Qyang, Y., Zhang, X., Li, X., Rosenfeld, M. G., Chen, J. and Evans, S. (2005). T-box genes coordinate regional rates of proliferation and regional specification during cardiogenesis. *Development* **132**, 2475-2487.
Cai, X., Nomura-Kitabayashi, A., Cai, W., Yan, J., Christoffels, V. M. and Cai, C. L. (2011). Myocardial Tbx20 regulates early atrioventricular canal formation and endocardial epithelial-mesenchymal transition via Bmp2. *Dev. Biol.* **360**, 381-390.
Camenisch, T. D., Spicer, A. P., Brehm-Gibson, T., Biesterfeldt, J., Augustine, M. L., Calabro, A., Jr, Kubalak, S., Klewer, S. E. and McDonald, J. A. (2000). Disruption of hyaluronan synthase-2 abrogates normal cardiac morphogenesis and hyaluronan-mediated transformation of epithelium to mesenchyme. *J. Clin. Invest.* **106**, 349-360.
Chakraborty, S., Combs, M. D. and Yutzey, K. E. (2010). Transcriptional regulation of heart valve progenitor cells. *Pediatr. Cardiol.* **31**, 414-421.
Chang, C. P., Neilson, J. R., Bayle, J. H., Gestwicki, J. E., Kuo, A., Stankunas, K., Graef, I. A. and Crabtree, G. R. (2004). A field of myocardial-endocardial NFAT signaling underlies heart valve morphogenesis. *Cell* **118**, 649-663.
Clevers, H. and Nusse, R. (2012). Wnt/β-catenin signaling and disease. *Cell* **149**, 1192-1205.
DasGupta, R. and Fuchs, E. (1999). Multiple roles for activated LEF/TCF transcription complexes during hair follicle development and differentiation. *Development* **126**, 4557-4568.
de la Pompa, J. L., Timmerman, L. A., Takimoto, H., Yoshida, H., Elia, A. J., Samper, E., Potter, J., Wakeham, A., Marengere, L., Langille, B. L. et al. (1998). Role of the NF-ATc transcription factor in morphogenesis of cardiac valves and septum. *Nature* **392**, 182-186.
de Lange, F. J., Moorman, A. F., Anderson, R. H., Männer, J., Soufan, A. T., de Gier-de Vries, C., Schneider, M. D., Webb, S., van den Hoff, M. J. and Christoffels, V. M. (2004). Lineage and morphogenetic analysis of the cardiac valves. *Circ. Res.* **95**, 645-654.
Driegen, S., Ferreira, R., van Zon, A., Strouboulis, J., Jaegle, M., Grosveld, F., Philipsen, S. and Meijer, D. (2005). A generic tool for biotinylation of tagged proteins in transgenic mice. *Transgenic Res.* **14**, 477-482.
Dupuis, L. E., McCulloch, D. R., McGarity, J. D., Bahan, A., Wessels, A., Weber, D., Diminich, A. M., Nelson, C. M., Apte, S. S. and Kern, C. B. (2011). Altered versican cleavage in ADAMTS5 deficient mice; a novel etiology of myxomatous valve disease. *Dev. Biol.* **357**, 152-164.
Farley, F. W., Soriano, P., Steffen, L. S. and Dymecki, S. M. (2000). Widespread recombinase expression using FLPeR (flipper) mice. *Genesis* **28**, 106-110.
Gessert, S. and Kühl, M. (2010). The multiple phases and faces of wnt signaling during cardiac differentiation and development. *Circ. Res.* **107**, 186-199.
Greulich, F., Rudat, C. and Kispert, A. (2011). Mechanisms of T-box gene function in the developing heart. *Cardiovasc. Res.* **91**, 212-222.
Griffin, K. J., Stoller, J., Gibson, M., Chen, S., Yelon, D., Stainier, D. Y. and Kimelman, D. (2000). A conserved role for H15-related T-box transcription factors in zebrafish and Drosophila heart formation. *Dev. Biol.* **218**, 235-247.
He, A. and Pu, W. T. (2010). Genome-wide location analysis by pull down of in vivo biotinylated transcription factors. *Curr. Protoc. Mol. Biol.* Chapter 21, 92:21.20.1-21.20.15.
Hinton, R. B. and Yutzey, K. E. (2011). Heart valve structure and function in development and disease. *Annu. Rev. Physiol.* **73**, 29-46.
Hinton, R. B., Jr, Lincoln, J., Deutsch, G. H., Osinska, H., Manning, P. B., Benson, D. W. and Yutzey, K. E. (2006). Extracellular matrix remodeling and organization in developing and diseased aortic valves. *Circ. Res.* **98**, 1431-1438.
Iio, A., Koide, M., Hidaka, K. and Morisaki, T. (2001). Expression pattern of novel chick T-box gene, Tbx20. *Dev. Genes Evol.* **211**, 559-562.
Jain, R., Engleka, K. A., Rentschler, S. L., Manderfield, L. J., Li, L., Yuan, L. and Epstein, J. A. (2011). Cardiac neural crest orchestrates remodeling and functional maturation of mouse semilunar valves. *J. Clin. Invest.* **121**, 422-430.
Jiao, K., Kulessa, H., Tompkins, K., Zhou, Y., Batts, L., Baldwin, H. S. and Hogan, B. L. (2003). An essential role of Bmp4 in the atrioventricular septation of the mouse heart. *Genes Dev.* **17**, 2362-2367.
Jiao, K., Langworthy, M., Batts, L., Brown, C. B., Moses, H. L. and Baldwin, H. S. (2006). Tgfbeta signaling is required for atrioventricular cushion mesenchyme remodeling during in vivo cardiac development. *Development* **133**, 4585-4593.
Kim, J., Cantor, A. B., Orkin, S. H. and Wang, J. (2009). Use of in vivo biotinylation to study protein-protein and protein-DNA interactions in mouse embryonic stem cells. *Nat. Protoc.* **4**, 506-517.
Kirk, E. P., Sunde, M., Costa, M. W., Rankin, S. A., Wolstein, O., Castro, M. L., Butler, T. L., Hyun, C., Guo, G., Otway, R. et al. (2007). Mutations in cardiac T-box factor gene TBX20 are associated with diverse cardiac pathologies, including defects of septation and valvulogenesis and cardiomyopathy. *Am. J. Hum. Genet.* **81**, 280-291.
Kraus, F., Haenig, B. and Kispert, A. (2001). Cloning and expression analysis of the mouse T-box gene tbx20. *Mech. Dev.* **100**, 87-91.
Kruithof, B. P., Krawitz, S. A. and Gaussin, V. (2007). Atrioventricular valve development during late embryonic and postnatal stages involves condensation and extracellular matrix remodeling. *Dev. Biol.* **302**, 208-217.
Liebner, S., Cattelino, A., Gallini, R., Rudini, N., Iurlaro, M., Piccolo, S. and Dejana, E. (2004). Beta-catenin is required for endothelial-mesenchymal transformation during heart cushion development in the mouse. *J. Cell Biol.* **166**, 359-367.
Lin, C. J., Lin, C. Y., Chen, C. H., Zhou, B. and Chang, C. P. (2012). Partitioning the heart: mechanisms of cardiac septation and valve development. *Development* **139**, 3277-3299.
Liu, C., Shen, A., Li, X., Jiao, W., Zhang, X. and Li, Z. (2008). T-box transcription factor TBX20 mutations in Chinese patients with congenital heart disease. *Eur. J. Med. Genet.* **51**, 580-587.
Ma, L., Lu, M. F., Schwartz, R. J. and Martin, J. F. (2005). Bmp2 is essential for cardiac cushion epithelial-mesenchymal transition and myocardial patterning. *Development* **132**, 5601-5611.
Meins, M., Henderson, D. J., Bhattacharya, S. S. and Sowden, J. C. (2000). Characterization of the human TBX20 gene, a new member of the T-Box gene family closely related to the Drosophila H15 gene. *Genomics* **67**, 317-332.
Merscher, S., Funke, B., Epstein, J. A., Heyer, J., Puech, A., Lu, M. M., Xavier, R. J., Demay, M. B., Russell, R. G., Factor, S. et al. (2001). TBX1 is responsible for cardiovascular defects in velo-cardio-facial/DiGeorge syndrome. *Cell* **104**, 619-629.
Nadeau, M., Georges, R. O., Laforest, B., Yamak, A., Lefebvre, C., Beauregard, J., Paradis, P., Bruneau, B. G., Andelfinger, G. and Nemer, M. (2010). An endocardial pathway involving Tbx5, Gata4, and Nos3 required for atrial septum formation. *Proc. Natl. Acad. Sci. USA* **107**, 19356-19361.
Naiche, L. A., Harrelson, Z., Kelly, R. G. and Papaioannou, V. E. (2005). T-box genes in vertebrate development. *Annu. Rev. Genet.* **39**, 219-239.
O'Gorman, S., Dagenais, N. A., Qian, M. and Marchuk, Y. (1997). Protamine-Cre recombinase transgenes efficiently recombine target sequences in the male germ line of mice, but not in embryonic stem cells. *Proc. Natl. Acad. Sci. USA* **94**, 14602-14607.
Packham, E. A. and Brook, J. D. (2003). T-box genes in human disorders. *Hum. Mol. Genet.* **12** Spec No 1, R37-R44.
Park, E. J., Watanabe, Y., Smyth, G., Miyagawa-Tomita, S., Meyers, E., Klingensmith, J., Camenisch, T., Buckingham, M. and Moon, A. M. (2008). An FGF autocrine loop initiated in second heart field mesoderm regulates morphogenesis at the arterial pole of the heart. *Development* **135**, 3599-3610.
Person, A. D., Klewer, S. E. and Runyan, R. B. (2005). Cell biology of cardiac cushion development. *Int. Rev. Cytol.* **243**, 287-335.

Posch, M. G., Gramlich, M., Sunde, M., Schmitt, K. R., Lee, S. H., Richter, S., Kersten, A., Perrot, A., Panek, A. N., Al Khatib, I. H. et al. (2010). A gain-of-function TBX20 mutation causes congenital atrial septal defects, patent foramen ovale and cardiac valve defects. *J. Med. Genet.* **47**, 230-235.
Qian, L., Mohapatra, B., Akasaka, T., Liu, J., Ocorr, K., Towbin, J. A. and Bodmer, R. (2008). Transcription factor neuromancer/TBX20 is required for cardiac function in Drosophila with implications for human heart disease. *Proc. Natl. Acad. Sci. USA* **105**, 19833-19838.
Qiao, Y., Wanyan, H., Xing, Q., Xie, W., Pang, S., Shan, J. and Yan, B. (2012). Genetic analysis of the TBX20 gene promoter region in patients with ventricular septal defects. *Gene* **500**, 28-31.
Ranger, A. M., Grusby, M. J., Hodge, M. R., Gravallese, E. M., de la Brousse, F. C., Hoey, T., Mickanin, C., Baldwin, H. S. and Glimcher, L. H. (1998). The transcription factor NF-ATc is essential for cardiac valve formation. *Nature* **392**, 186-190.
Rivera-Feliciano, J., Lee, K. H., Kong, S. W., Rajagopal, S., Ma, Q., Springer, Z., Izumo, S., Tabin, C. J. and Pu, W. T. (2006). Development of heart valves requires Gata4 expression in endothelial-derived cells. *Development* **133**, 3607-3618.
Shelton, E. L. and Yutzey, K. E. (2007). Tbx20 regulation of endocardial cushion cell proliferation and extracellular matrix gene expression. *Dev. Biol.* **302**, 376-388.
Singh, M. K., Christoffels, V. M., Dias, J. M., Trowe, M. O., Petry, M., Schuster-Gossler, K., Bürger, A., Ericson, J. and Kispert, A. (2005). Tbx20 is essential for cardiac chamber differentiation and repression of Tbx2. *Development* **132**, 2697-2707.
Snider, P., Hinton, R. B., Moreno-Rodriguez, R. A., Wang, J., Rogers, R., Lindsley, A., Li, F., Ingram, D. A., Menick, D., Field, L. et al. (2008). Periostin is required for maturation and extracellular matrix stabilization of noncardiomyocyte lineages of the heart. *Circ. Res.* **102**, 752-760.
Soriano, P. (1999). Generalized lacZ expression with the ROSA26 Cre reporter strain. *Nat. Genet.* **21**, 70-71.
Stankunas, K., Ma, G. K., Kuhnert, F. J., Kuo, C. J. and Chang, C. P. (2010). VEGF signaling has distinct spatiotemporal roles during heart valve development. *Dev. Biol.* **347**, 325-336.
Stennard, F. A., Costa, M. W., Lai, D., Biben, C., Furtado, M. B., Solloway, M. J., McCulley, D. J., Leimena, C., Preis, J. I., Dunwoodie, S. L. et al. (2005). Murine T-box transcription factor Tbx20 acts as a repressor during heart development, and is essential for adult heart integrity, function and adaptation. *Development* **132**, 2451-2462.
Takeuchi, J. K., Mileikovskaia, M., Koshiba-Takeuchi, K., Heidt, A. B., Mori, A. D., Arruda, E. P., Gertsenstein, M., Georges, R., Davidson, L., Mo, R. et al. (2005). Tbx20 dose-dependently regulates transcription factor networks required for mouse heart and motoneuron development. *Development* **132**, 2463-2474.
Timmerman, L. A., Grego-Bessa, J., Raya, A., Bertrán, E., Pérez-Pomares, J. M., Díez, J., Aranda, S., Palomo, S., McCormick, F., Izpisúa-Belmonte, J. C. et al. (2004). Notch promotes epithelial-mesenchymal transition during cardiac development and oncogenic transformation. *Genes Dev.* **18**, 99-115.
Todorovic, V., Finnegan, E., Freyer, L., Zilberberg, L., Ota, M. and Rifkin, D. B. (2011). Long form of latent TGF-β binding protein 1 (Ltbp1L) regulates cardiac valve development. *Dev. Dyn.* **240**, 176-187.
van Amerongen, R. and Nusse, R. (2009). Towards an integrated view of Wnt signaling in development. *Development* **136**, 3205-3214.
van Genderen, C., Okamura, R. M., Fariñas, I., Quo, R. G., Parslow, T. G., Bruhn, L. and Grosschedl, R. (1994). Development of several organs that require inductive epithelial-mesenchymal interactions is impaired in LEF-1-deficient mice. *Genes Dev.* **8**, 2691-2703.
Wang, J., Sinha, T. and Wynshaw-Boris, A. (2012). Wnt signaling in mammalian development: lessons from mouse genetics. *Cold Spring Harb. Perspect. Biol.* **4**, a007963.
Wilkinson, D. G. (1992). *In Situ Hybridization: A Practical Approach*. New York, NY: Oxford University Press.
Wirrig, E. E. and Yutzey, K. E. (2011). Transcriptional regulation of heart valve development and disease. *Cardiovasc. Pathol.* **20**, 162-167.
Wu, B., Wang, Y., Lui, W., Langworthy, M., Tompkins, K. L., Hatzopoulos, A. K., Baldwin, H. S. and Zhou, B. (2011). Nfatc1 coordinates valve endocardial cell lineage development required for heart valve formation. *Circ. Res.* **109**, 183-192.
Wu, B., Zhang, Z., Lui, W., Chen, X., Wang, Y., Chamberlain, A. A., Moreno-Rodriguez, R. A., Markwald, R. R., O'Rourke, B. P., Sharp, D. J. et al. (2012). Endocardial cells form the coronary arteries by angiogenesis through myocardial-endocardial VEGF signaling. *Cell* **151**, 1083-1096.
Yu, S., Crawford, D., Tsuchihashi, T., Behrens, T. W. and Srivastava, D. (2011). The chemokine receptor CXCR7 functions to regulate cardiac valve remodeling. *Dev. Dyn.* **240**, 384-393.
Zhang, J., Chang, J. Y., Huang, Y., Lin, X., Luo, Y., Schwartz, R. J., Martin, J. F. and Wang, F. (2010). The FGF-BMP signaling axis regulates outflow tract valve primordium formation by promoting cushion neural crest cell differentiation. *Circ. Res.* **107**, 1209-1219.
Zhou, B., Wu, B., Tompkins, K. L., Boyer, K. L., Grindley, J. C. and Baldwin, H. S. (2005). Characterization of Nfatc1 regulation identifies an enhancer required for gene expression that is specific to pro-valve endocardial cells in the developing heart. *Development* **132**, 1137-1146.
Zimmerman, Z. F., Moon, R. T. and Chien, A. J. (2012). Targeting Wnt pathways in disease. *Cold Spring Harb. Perspect. Biol.* **4**, a008086.

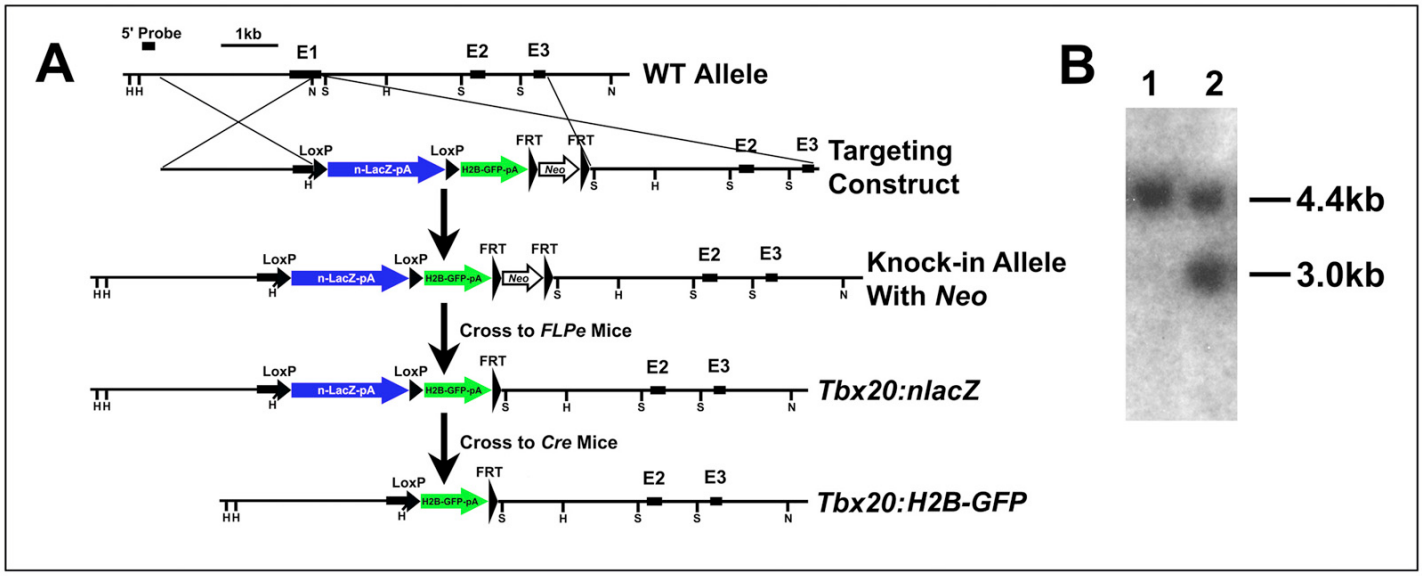

Fig. S1. Generation of *Tbx20*^{nlacZ} and *Tbx20*^{H2BGFP} knock-in mice. (**A**) The *Tbx20*$^{nlacZ/H2BGFP}$ mouse model. A *LoxP-nlacZ-polyA-LoxP-H2BGFP-polyA* cassette is introduced into exon 1 of *Tbx20*. Bars indicate exons. H, *Hin*dIII; S, *Sma*I. Mice with a knock-in allele derived from positive ESCs are crossed to *Flippase* mice to remove the *Neo* cassette. *Tbx20*^{H2BGFP} mice are obtained by crossing *Tbx20*$^{nlacZ/H2BGFP}$ mice with *Protamine-Cre* mice. (**B**) Southern blot of ESC DNA digested with *Hin*dIII hybridized with a genomic fragment external to the 5′ targeting construct, showing the wild-type band at 4.4 kb and the recombinant band at 3.0 kb.

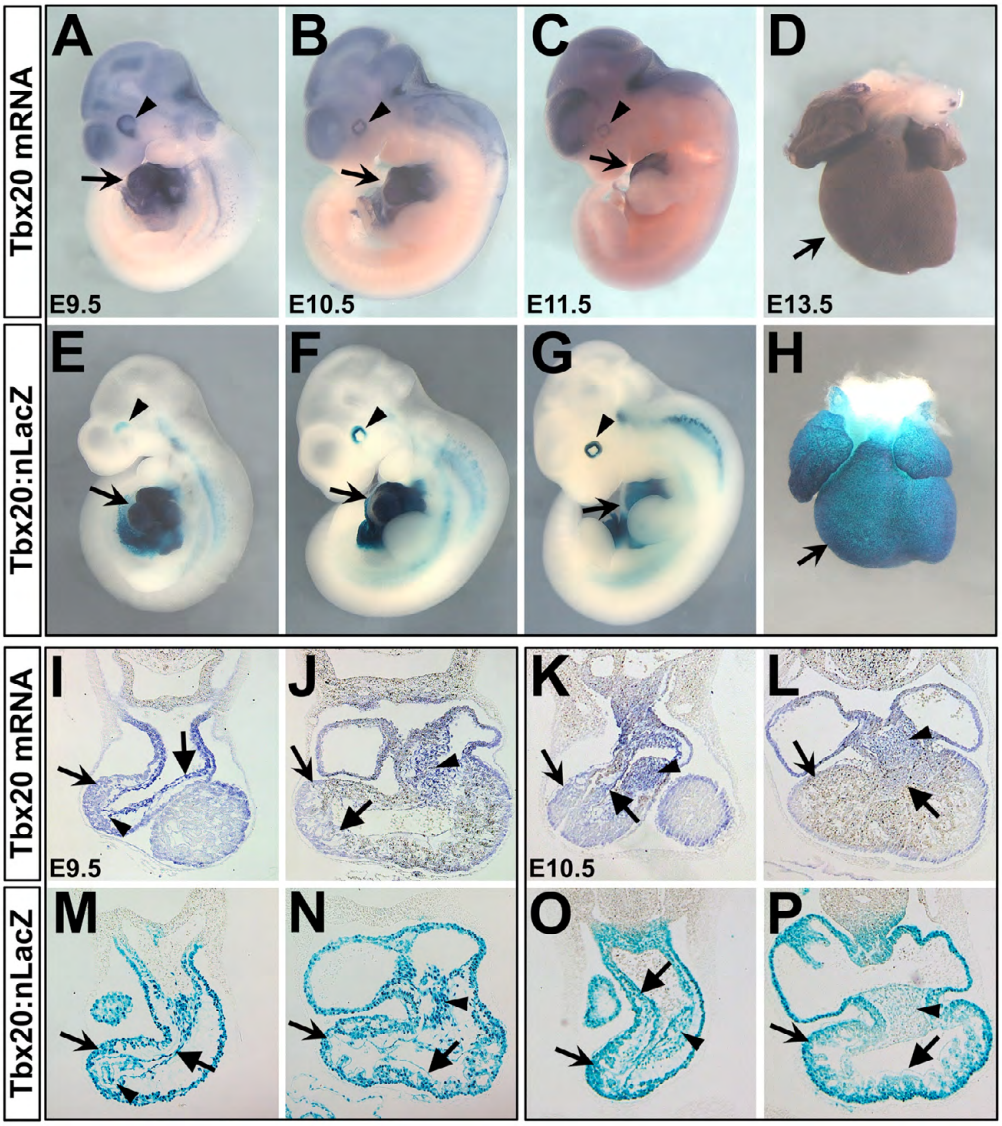

Fig. S2. *Tbx20*^{nlacZ} recapitulates the endogenous *Tbx20* expression pattern. (**A-D**) Whole-mount RNA *in situ* hybridization of *Tbx20* at E9.5 (A), E10.5 (B), E11.5 (C) and E13.5 (D). (**E-H**) Whole-mount X-Gal staining of *Tbx20*^{nlacZ} embryos at E9.5 (E), E10.5 (F), E11.5 (G) and E13.5 (H). Arrows indicate the heart region and arrowheads indicate the optic vesicle. (**I-L**) *Tbx20* RNA *in situ* hybridization on heart sections at E9.5 (I,J) and E10.5 (K,L). (**M-P**) X-Gal staining of *Tbx20*^{nlacZ} heart sections at E9.5 (M,N) and E10.5 (O,P). *Tbx20*^{nlacZ} faithfully recapitulates endogenous *Tbx20* mRNA expression in the heart, including myocardium (notched arrows), endocardium (unnotched arrows) and cushion mesenchyme (arrowheads).

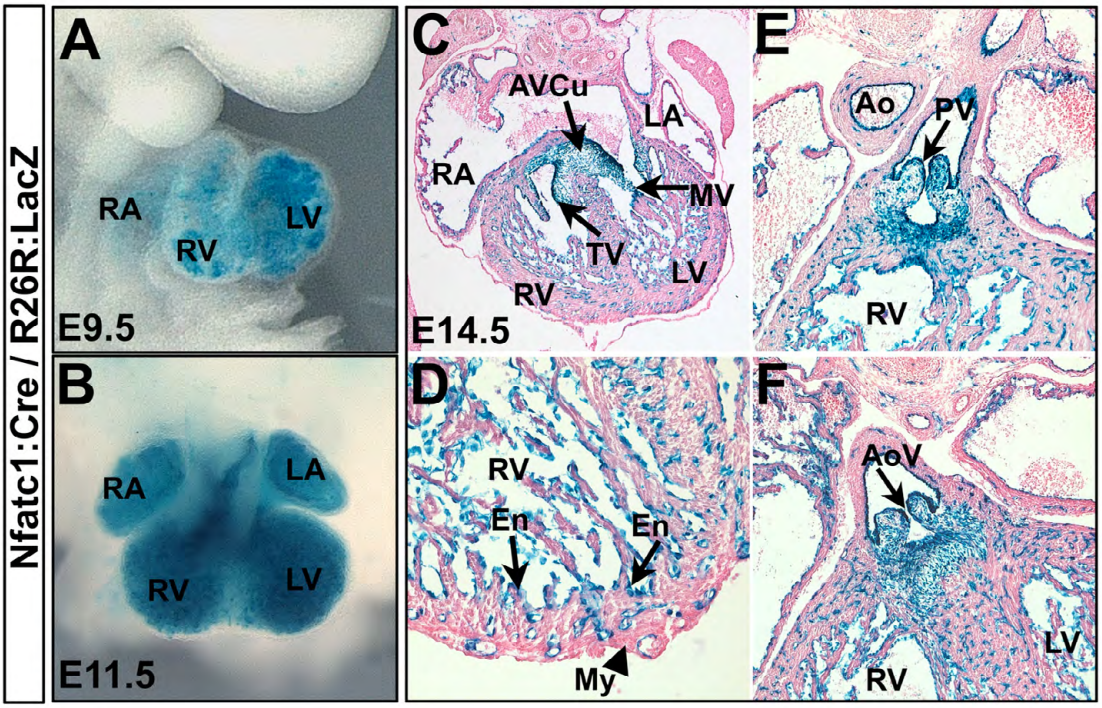

Fig. S3. *Nfatc1*^{Cre} lineage in endocardium and mesenchyme. (**A**,**B**) Whole-mount X-Gal staining of *Nfatc1*$^{Cre/+}$;*R26R*^{lacZ} hearts at E9.5 (A) and E11.5 (B). (**C-F**) X-Gal staining of heart sections at E14.5. *Nfatc1*$^{Cre/+}$ derivatives are found in endocardium (arrows in D) and cushion mesenchyme (arrows in C,E,F), but not myocardium (arrowhead in D). En, endocardium; My, myocardium.

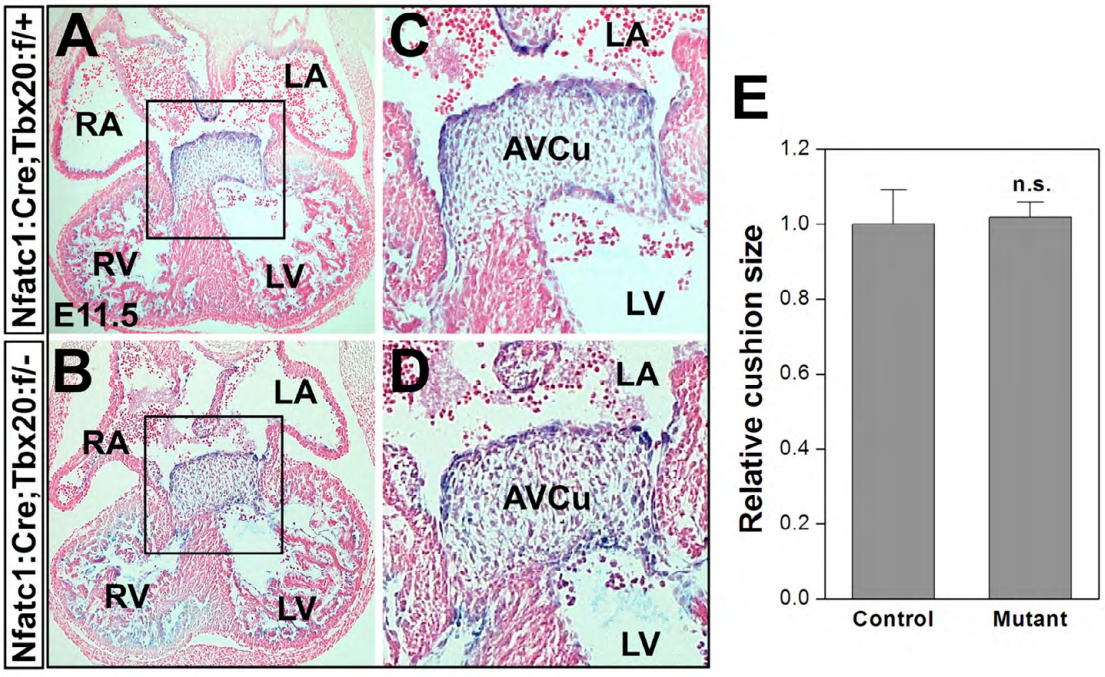

Fig. S4. Normal atrioventricular cushion formation in *Tbx20* CKO embryos at E11.5. (**A-D**) Transverse sections of *Tbx20* CKO mutant and control hearts at E11.5. C,D are higher magnification images for A,B in the atrioventricular cushion region (boxed), respectively. (**E**) Relative atrioventricular cushion size. The mutant atrioventricular cushion size is normal at E11.5. n.s., not significant.

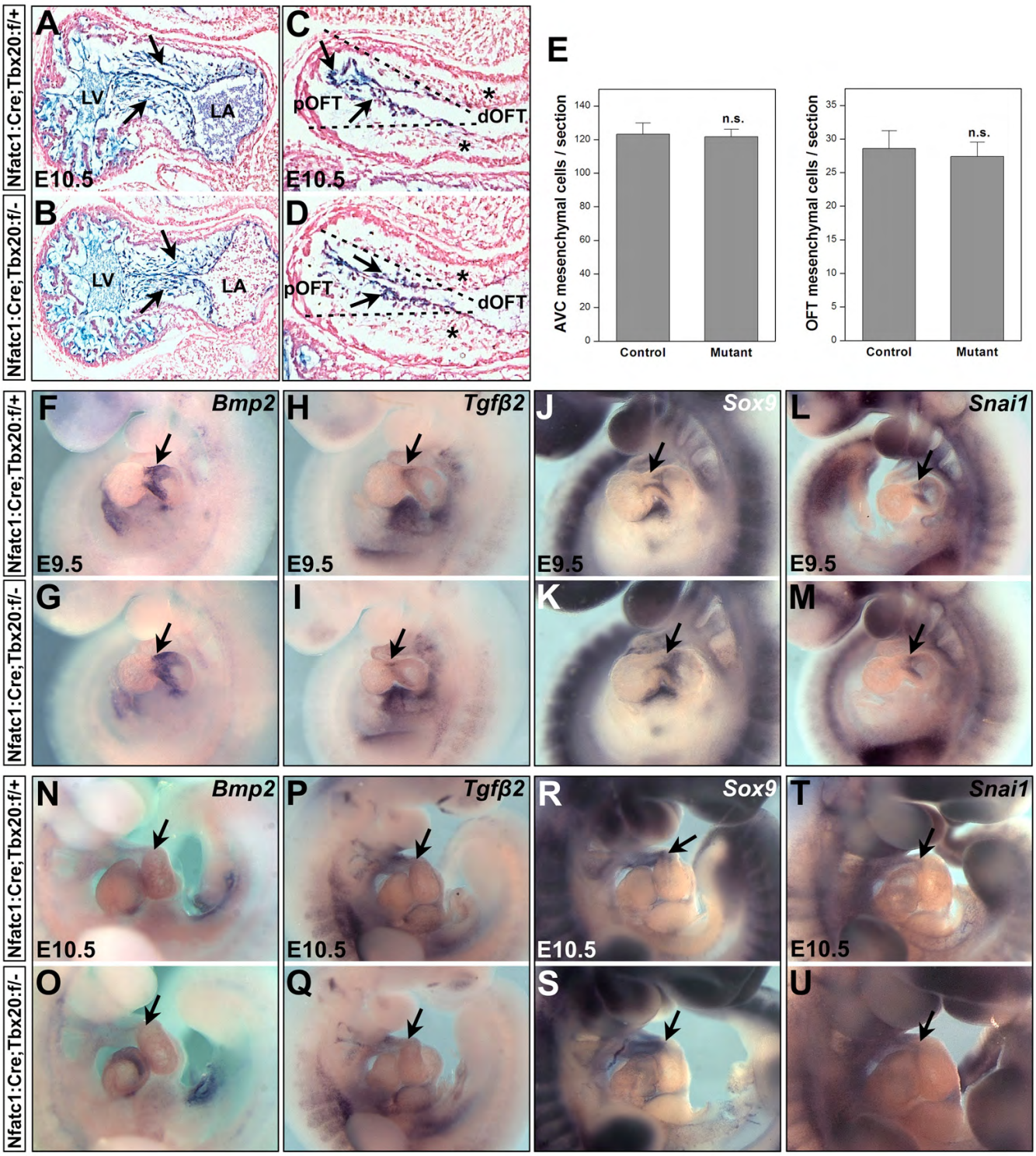

Fig. S5. Endocardial *Tbx20* is not required for early EMT initiation. (**A-D**) Sagittal sections of control (*Nfatc1*$^{Cre/+}$;*Tbx20*$^{f/+}$;*R26R*^{lacZ}) and mutant (*Nfatc1*$^{Cre/+}$;*Tbx20*$^{f/-}$;*R26R*^{lacZ}) hearts at E10.5. Embryos containing one copy of the *R26R*^{lacZ} allele are to detect *Nfatc1*^{Cre} progeny in which the *Tbx20* floxed allele is recombined. X-Gal staining shows *Nfatc1*^{Cre} lineage cells including endocardium and cushion mesenchyme. Arrows indicate mesenchymal cells. In OFT, mesenchymal cells derived from the endocardial lineage are located in the proximal OFT (pOFT). Mesenchymal cells in the distal OFT (dOFT) originate from neural crest and are X-Gal staining negative (asterisk). Dashed lines indicate the junctions between the *Nfatc1*^{Cre} lineage and the neural crest lineage. (**E**) Statistical analysis reveals no significant difference in the number of mesenchymal cells in AVC and OFT regions of mutant and control hearts at E10.5. n.s., not significant. (**F-M**) RNA *in situ* hybridization of EMT related genes in the AVC at E9.5. Arrows indicate the AVC region. (**N-U**) RNA *in situ* hybridization of EMT related genes in the OFT at E10.5. No differential expression is found. Arrows indicate the OFT region. OFT, outflow tract; AVC, atrioventricular canal.

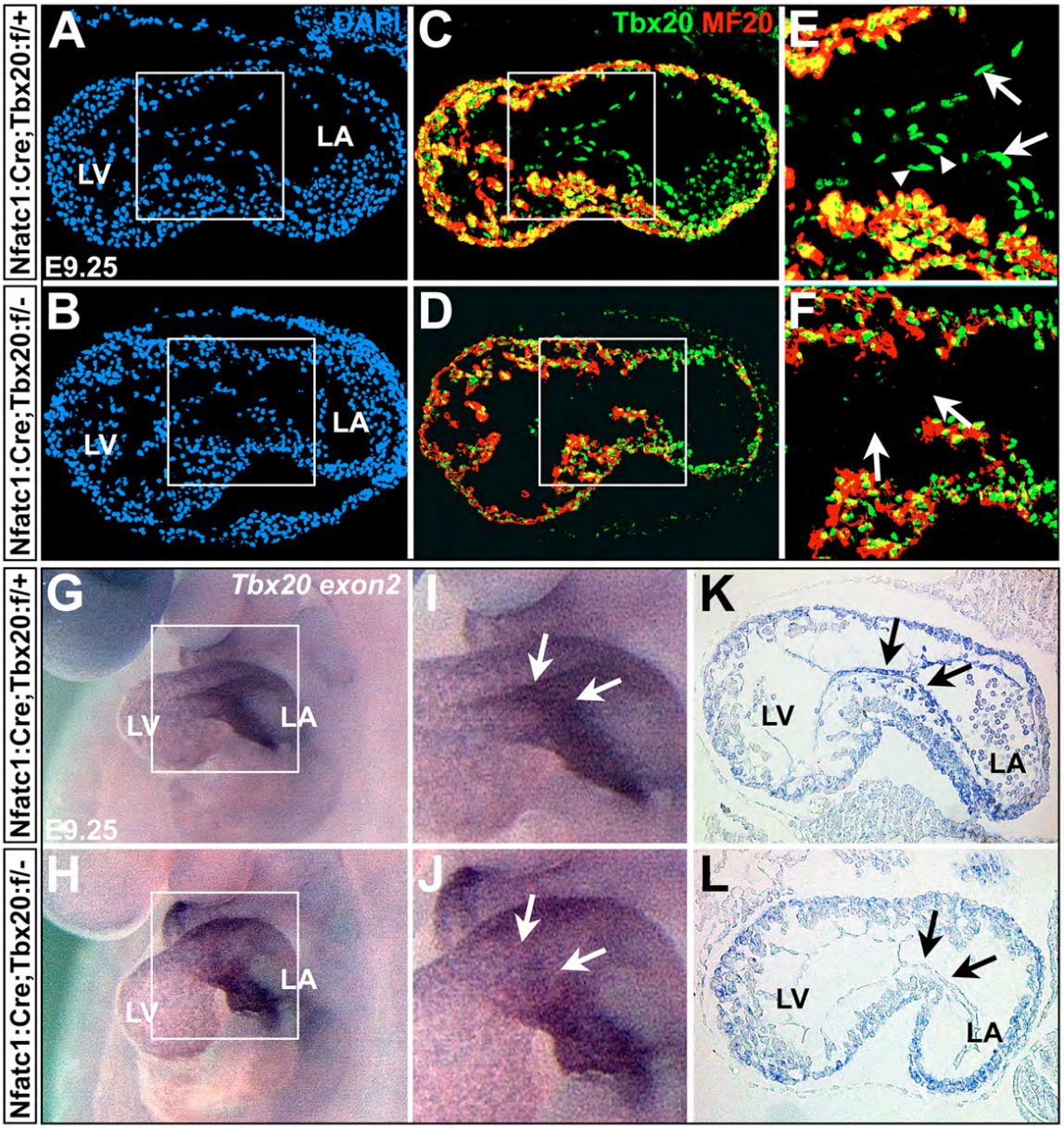

Fig. S6. Efficient and specific disruption of *Tbx20* by *Nfatc1*^{Cre} in the endocardial and cushion mesenchymal cells of *Tbx20* CKO embryos. (**A-F**) Co-immunostaining of Tbx20 (green) and with MF20 (red) in control (A,C,E) and mutant (B,D,F) hearts at E9.25. MF20 co-stains with Tbx20 in the myocardium (yellow). E,F are higher magnification images for C,D in the AVC region (boxed), respectively. In the control heart (E), Tbx20 is highly expressed in the endocardial (arrows) and mesenchymal (arrowheads) cells. Tbx20 immunostaining signals are barely detected in the endocardial and mesenchymal cells in the mutant at E9.25 (arrows in F). (**G-L**) Whole-mount RNA *in situ* hybridization of *Tbx20* exon 2 in control (G,I) and mutant (H,J) at E9.25. I,J are higher magnification images for G,H in the AVC region (boxed), respectively. Sections of the AVC region are shown in K and L. *Tbx20* exon 2 expression can be detected in the AVC endocardial and mesenchymal cells in the control (arrows in I,K) but not in these cells in the mutant (arrows in J,L).

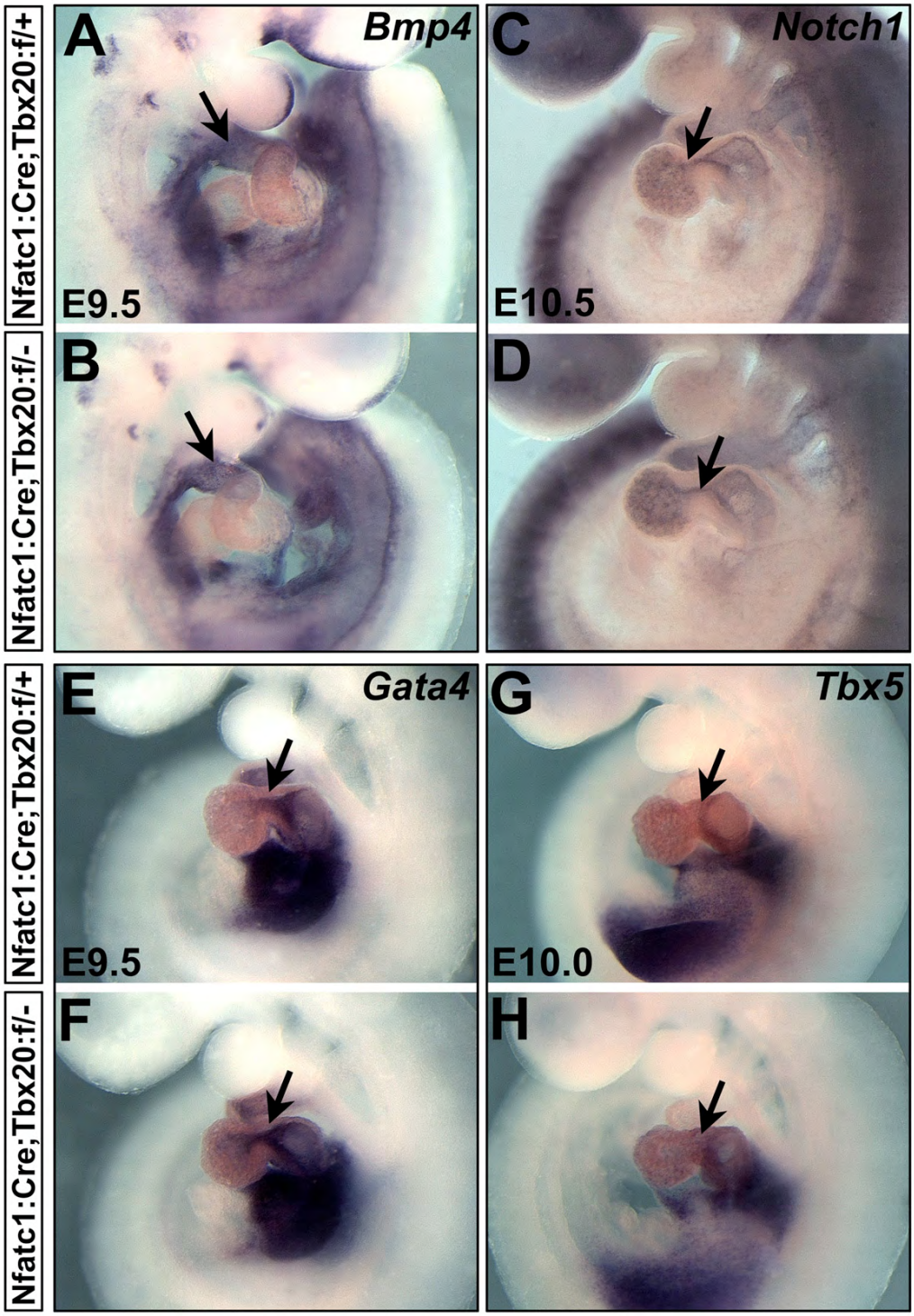

Fig. S7. Genes essential for early endocardial cushion development are expressed normally in *Tbx20* CKO embryos. (**A-H**) RNA *in situ* hybridization indicates that genes crucial for endocardial cushion and valve formation, including *Bmp4* (A,B), *Notch1* (C,D), *Gata4* (E,F) and *Tbx5* (G,H), are expressed normally in the mutant hearts (arrows).

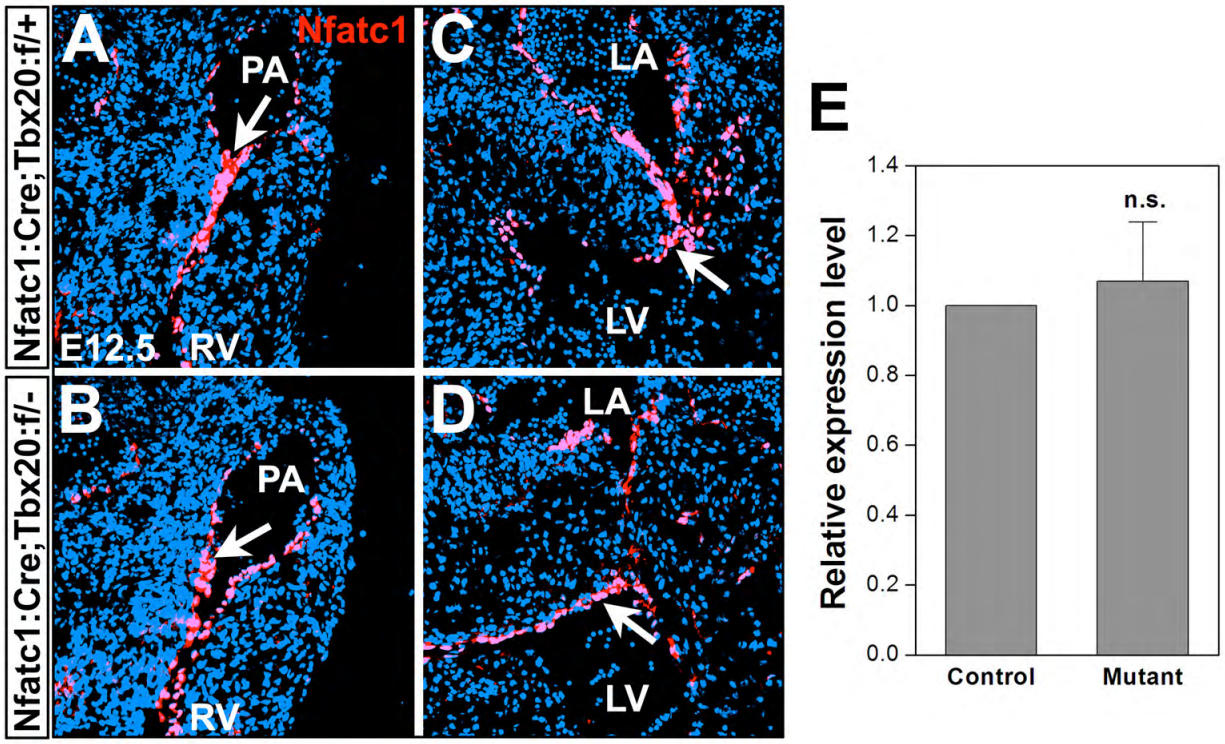

Fig. S8. Nfatc1 is expressed normally in *Tbx20* CKO heart. (**A-D**) Immunostaining of Nfatc1 (red) in control (A,C) and mutant (B,D) hearts at E12.5. Nfatc1 is expressed normally in valve endocardial cells in both pulmonary valve (arrows in A,B) and mitral valve (arrows in C,D). (**E**) Relative expression of *Nfatc1* in E12.5 control and mutant heart as determined by RT-qPCR. n.s., not significant. PA, pulmonary artery.

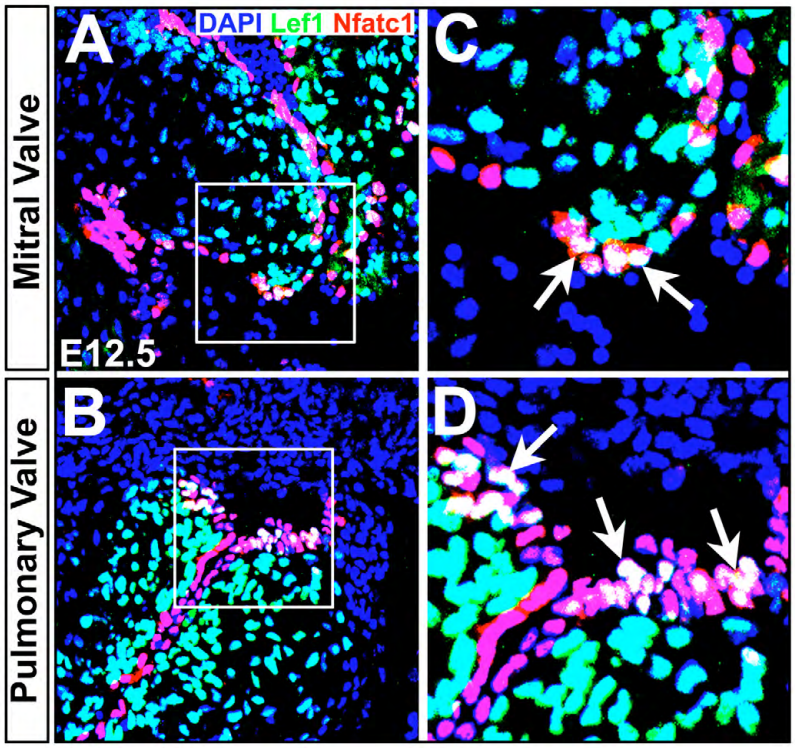

Fig. S9. Lef1 is co-expressed with Nfatc1 in cushion endocardial cells. (**A-D**) Immunostaining of Lef1 (green) and Nfatc1 (red) in the mitral valve (A,C) and pulmonary valve (B,D) at E12.5. Nfatc1 marks valve endocardial cells. C,D are higher magnification images for A,B in the valve region (boxed), respectively. Arrows indicate co-staining of Lef1 and Nfatc1 in valve endocardial cells (white).

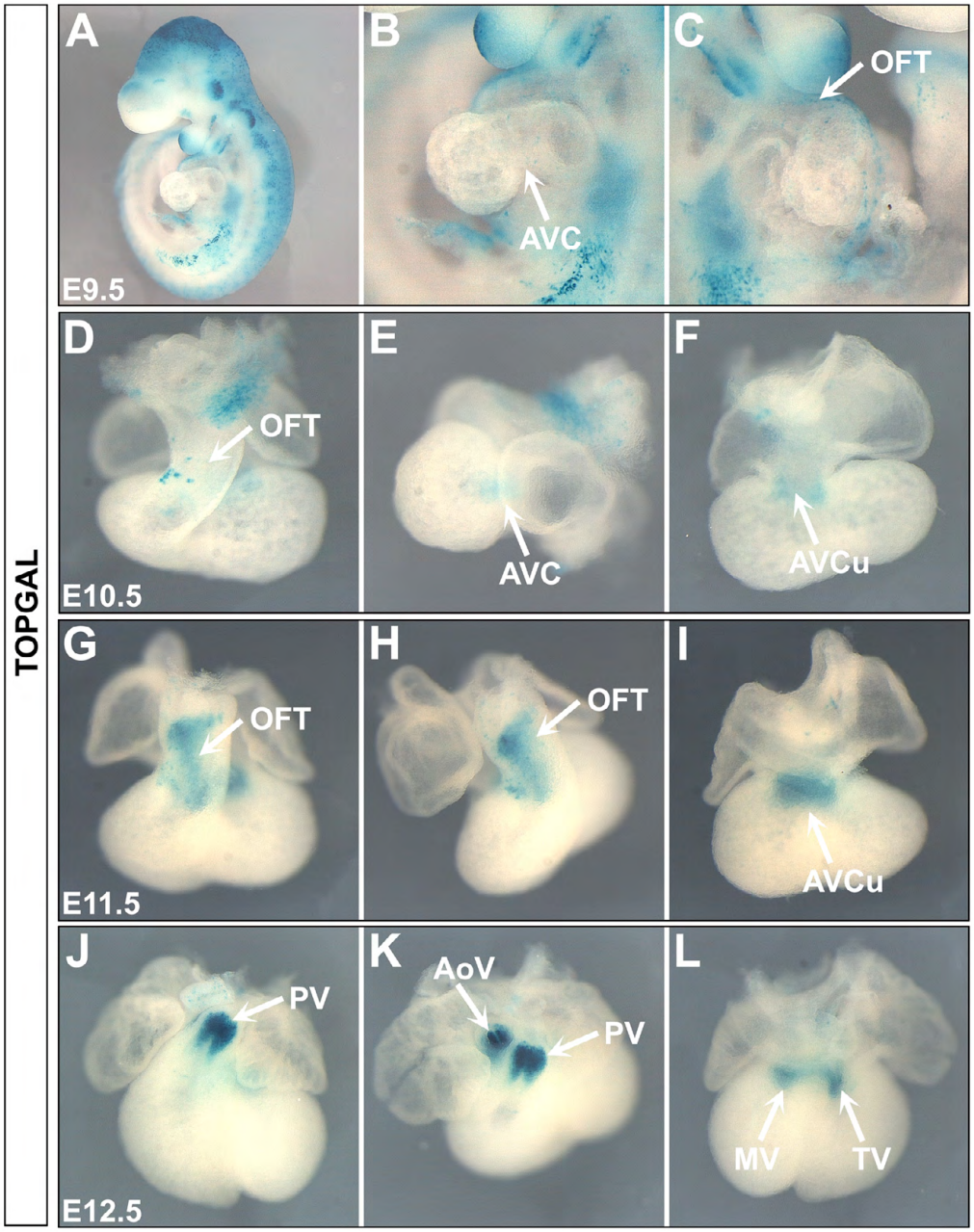

Fig. S10. Wnt/β-catenin signaling activity in the heart determined in *TOPGAL* mice. (**A-L**) Whole-mount X-Gal staining of *TOPGAL* mouse hearts at E9.5 (A-C), E10.5 (D-F), E11.5 (G-I) and E12.5 (J-L). Arrows indicate that active Wnt/β-catenin signals are specifically located in the primitive endocardial cushion and valve regions from E10.5 to E12.5. OFT, outflow tract; AVC, atrioventricular canal; AVCu, atrioventricular cushion; PV/AoV, pulmonary/aortic valve; TV/MV, tricuspid/mitral valve.

Table S1. Primers

	Forward (5'-3')	Reverse (5'-3')
RT-qPCR		
Actb	TGAACCCTAAGGCCAACCGTGAAA	CAGGATGGCGTGAGGGAGAGCATAG
Acan	GTGATGATCTGGCATGAGAGAGG	CACCAGGGAGCTGATCTCG
Col1a1	TGGTTTGGAGAGAGCATGACC	GATCCCTGGAGGAGCAGG
Has2	CACAGCCTTCAGAGCACTGG	GCTGAGGAAGGAGATCCAGG
lacZ	GCCCATCTACACCAACGTAACC	AGTAACAACCCGTCGGATTCTC
Lef1	ACGCTAAAGGAGAGTGCAGC	ATTGTCTCGCGCTGACCA
Mmp2	CTTTGCAGGAGACAAGTTCTGG	AATAAGCACCCTTGAAGAAGTAGC
Mmp9	CCATGCACTGGGCTTAGATCA	GGCCTTGGGTCAGGCTTAGA
Mmp13	GGAAGACCCTCTTCTTCTCT	TCATAGACAGCATCTACTTTGTT
Postn	AATGCTGCCCTGGCTATATG	GTAGTGGCTCCCACAATGC
Vcan	TCCTGATTGGCATTAGTGAAGAGT	CTGGTCTCCGCTGTATCCAG
Wnt4	GGGCACTCATGAATCTTCACAAC	GCCAGCACGTCTTTACCTC
Wnt7b	CGTCTTCGGGCAAGAACTCC	GGTCACAGCCACAATTGCTCA
Wnt9b	GAGGAAGCAAGGACCTGAGG	GGGAGAGCTGCTTCCAACAG
ChIP-PCR		
P1	CCACGTGGCTGCAAAATCTCTA	
P2	GCTGTTGGTTTTTCTCCTCCTG	
P3	AGAGTCACAACTCTTCTGTTTGC	
P4	CTCTTCTTCTCTTGCCGACC	
***Lef1* promoter fragments**		
3.9 kb	GGACAGTGTTCCCTCCACCC	CCCTCGGTCAAAGCAAAGAGCTGC
2.9 kb	AATTAAATCACATCAAAACGCCCC	CCCTCGGTCAAAGCAAAGAGCTGC
1.7 kb	CAACCACGTCCTATGCAGCAAACC	CCCTCGGTCAAAGCAAAGAGCTGC

Table S2. Genes identified by DEGseq R packages and differentially expressed >1.5-fold.

Download Table S2

Table S3. Significant canonical pathways identified by ingenuity pathway analysis.

Download Table S3

Table S4. GO terms significantly enriched among the differentially expressed genes.

Download Table S4